Biochimica et Biophysica Acta 1848 (2015) 781–796

Contents lists available at ScienceDirect

Biochimica et Biophysica Acta

journal homepage: www.elsevier.com/locate/bbamem

TRH-receptor mobility and function in intact and cholesterol-depleted plasma membrane of HEK293 cells stably expressing TRH-R-eGFP

Jana Brejchová [a], Jan Sýkora [b], Pavel Ostašov [a], Ladislav Merta [a], Lenka Roubalová [a], Jiří Janáček [a], Martin Hof [b], Petr Svoboda [a,*]

[a] Institute of Physiology, Academy of Sciences of the Czech Republic v.v.i., Vídeňská 1083, 14220 Prague 4, Czech Republic
[b] J. Heyrovsky Institute of Physical Chemistry, Academy of Sciences of the Czech Republic v.v.i., Dolejškova 2155/3, 18223 Prague 8, Czech Republic

ARTICLE INFO

Article history:
Received 1 August 2014
Received in revised form 24 November 2014
Accepted 26 November 2014
Available online 6 December 2014

Keywords:
Cholesterol
TRH-R-eGFP mobility
FRAP
RICS
DPH fluorescence
G protein coupling

ABSTRACT

Here we investigated the effect of disruption of plasma membrane integrity by cholesterol depletion on thyrotropin-releasing hormone receptor (TRH-R) surface mobility in HEK293 cells stably expressing TRH-R-eGFP fusion protein (VTGP cells). Detailed analysis by fluorescence recovery after photobleaching (FRAP) in bleached spots of different sizes indicated that cholesterol depletion did not result in statistically significant alteration of mobile fraction of receptor molecules (M_f). The apparent diffusion coefficient (D_{app}) was decreased, but this decrease was detectable only under the special conditions of screening and calculation of FRAP data. Analysis of mobility of receptor molecules by raster image correlation spectroscopy (RICS) did not indicate any significant difference between control and cholesterol-depleted cells. Results of our FRAP and RICS experiments may be collectively interpreted in terms of a "membrane fence" model which regards the plasma membrane of living cells as compartmentalized plane where lateral diffusion of membrane proteins is limited to restricted areas by cytoskeleton constraints. Hydrophobic interior of plasma membrane, studied by steady-state and time-resolved fluorescence anisotropy of hydrophobic membrane probe DPH, became substantially more "fluid" and chaotically organized in cholesterol-depleted cells. Decrease of cholesterol level impaired the functional coupling between the receptor and the cognate G proteins of G_q/G_{11} family.
In conclusion: the presence of an unaltered level of cholesterol in the plasma membrane represents an obligatory condition for an optimum functioning of TRH-R signaling cascade. The decreased order and increased fluidity of hydrophobic membrane interior suggest an important role of this membrane area in TRH-R–$G_q/G_{11}\alpha$ protein coupling.

1. Introduction

Cholesterol plays an important role in the cell membrane organization. It regulates membrane fluidity, affects protein conformation and also functions as an essential constituent of the plasma membrane (PM) structures known as detergent resistant membrane domains (DRMs) [1–3]. These structures arising from PM after detergent extraction at 0 °C were found to be enriched in this highly hydrophobic membrane constituent together with lipids containing higher proportion of saturated fatty acids when compared with the rest of the membrane. Biophysical studies indicated a gel-like or liquid-ordered state of these structures [4]. DRMs were found to be enriched in signaling and regulatory molecules such as trimeric G-protein α subunits, various types of protein kinases and glycosylphosphatidylinositol (GPI)-anchored proteins [5–8], but the relative proportion of thyrotropin-releasing hormone receptor (TRH-R) in DRMs was very low [9]. No more than 1–3% of the total amount of the TRH-R originally present in PM was recovered in DRMs isolated from the HEK293 cells stably expressing this receptor.

We have also shown that treatment of HEK293 cells with cholesterol-depleting agent β-cyclodextrin (β-CDX) caused the degradation of DRMs and a change of their protein composition including specific decrease of the cognate G-protein α subunits, $G_s\alpha$ and $G_q\alpha/G_{11}\alpha$ [10,11]. TRH-induced stimulation of G-protein activity in isolated PM (measured as [^{35}S]GTPγS binding assay) as well as Ca^{2+}-response in intact cells

Abbreviations: BPM, bulk of plasma membranes; β-CDX, β-cyclodextrin; CLSM, confocal laser scanning microscopy; D_{app}, apparent diffusion coefficient; DPH, 1,6-diphenyl-1,3,5-hexatriene; DRMs/DIMs, detergent-resistant or detergent-insensitive membrane domains; DMEM, Dulbecco's modified Eagle's medium; eGFP, enhanced green fluorescent protein; FRAP, fluorescence recovery after photobleaching; G-proteins, heterotrimeric guanine nucleotide-binding regulatory proteins; $G_q/G_{11}\alpha$, G proteins stimulating phospholipase C in pertussis toxin-independent manner; $G_i1\alpha$, G protein inhibiting adenylyl cyclase activity in pertussis toxin-sensitive manner; GPCR, G-protein-coupled receptor; GPI, glycosylphosphatidylinositol; HEK, human embryonic kidney; M_f, mobile fraction of receptor molecules; PBS, phosphate-buffered saline; PM, plasma membrane (cell membrane); PMSF, phenylmethylsulfonyl fluoride; PNS, post-nuclear supernatant; r_{DPH}, anisotropy of DPH fluorescence; RICS, raster image correlation spectroscopy; ROI, region of interest; SLB, solubilization lysis buffer; TM, trans-membrane; VSV, vesicular stomatitis virus; TRH, thyrotropin-releasing hormone; TRH-R, thyrotropin-releasing hormone receptor; VSV-TRH-R-eGFP, N-terminally VSV-tagged form of TRH-R-eGFP fusion protein; VTGP cells, HEK293 cells stably expressing VSV-TRH-R-eGFP

* Corresponding author. Tel.: +420 241062478; fax: +420 24106 2488.
E-mail address: svobodap@biomed.cas.cz (P. Svoboda).

http://dx.doi.org/10.1016/j.bbamem.2014.11.029
0005-2736/

was severely deteriorated under such conditions [11]. The dose–response curves of the increase of intracellular calcium levels $[Ca^{2+}]_i$ were shifted by two orders of magnitude to the right, i.e., much higher TRH concentrations were needed to elicit the same $[Ca^{2+}]_i$ response. Furthermore, the decrease of cholesterol level was associated with redistribution of $G_q/G_{11}\alpha$ proteins at the cell surface as their immunofluorescence signal became stronger than in β-CDX-untreated cells. This change was interpreted as a release of $G_q/G_{11}\alpha$ proteins from previously more closely packed protein complexes, i.e. as loosening of previously more closely attached $G_q/G_{11}\alpha$ protein aggregates. Last but not the least, the characteristics of desensitization of $[Ca^{2+}]_i$ response in cells over-expressing $G_{11}\alpha$ protein were altered by β-CDX treatment indicating that the proper structural state of the plasma membrane is necessary for an optimum proceeding of desensitization of hormone response [12].

The data indicating the low amount of TRH-R in DRMs were surprising because numerous other G-protein-coupled receptors (GPCRs), including α_1- and β_2-adrenergic, thyrothropin, bradykinin, endothelin, P2Y purinergic, serotonin, muscarinic and adenosine receptors have been detected in DRMs in much higher proportions [10,13–17]. Therefore, the goal of our present study was to evaluate the structural and dynamic properties of TRH-R molecule in the plasma membrane of living cells. For this aim we used the HEK293 cell line stably expressing TRH-R-eGFP fusion protein (VTGP cells) [18,19].

Cholesterol depletion, induced by pre-incubation of VTGP cells with β-CDX, served as an experimental tool for alteration of plasma membrane structure and function and, more specifically, for degradation of membrane domains/rafts. The alteration of lateral diffusion of TRH-R-eGFP molecules in the plasma membrane was tested by fluorescence recovery after photobleaching (FRAP) and raster image correlation spectroscopy (RICS). Hydrophobic lipid matrix of plasma membrane was characterized by steady-state and time-resolved fluorescence anisotropy of the hydrophobic membrane probe diphenylhexatriene (DPH). The effect of cholesterol depletion on functional coupling of TRH-R-eGFP with cognate G-proteins was determined by [^{35}S]GTPγS binding assay followed by $G_q/G_{11}\alpha$-oriented immunoprecipitation.

2. Materials and methods

2.1. Chemicals

Newborn calf serum (NCS) was purchased from Invitrogen-Gibco. Amplex Red Cholesterol assay kit and 1,6-diphenyl-1,3,5-hexatriene (DPH) were from Invitrogen-Molecular probes (Eugene, Oregon). All other chemicals were either from Sigma or Gibco and were of the highest purity available.

2.2. Cell culture

HEK293 cells stably expressing VSV-epitope and eGFP-tagged version of thyrotropin-releasing hormone receptor (VTGP cells) were grown in Dulbecco's modified Eagle's medium (DMEM) supplemented with 2 mM (0.292 g/l) L-glutamine and 8% newborn calf serum in humidified atmosphere containing 5% CO_2 at 37 °C as described before by Drmota et al. [18]. Geneticin (800 μg/ml) was included in the course of cell cultivation to maintain appropriate selection pressure. The cells were grown to 60–80% confluency in tissue culture flasks impregnated with 2% gelatine. When performing confocal laser scanning microscopy (CLSM) or FRAP experiments, the cells were grown for 48 h on glass cover-slips coated with 0.1 mg/ml poly-L-lysine.

2.3. Cholesterol depletion

In order to deplete cholesterol from the cell membrane, 10 mM β-cyclodextrin dissolved in serum free DMEM was added to a pre-confluent (70–80%) culture of VTGP cells at time zero. After 30 min at 37 °C, β-CDX-containing incubation medium was withdrawn and replaced with serum free DMEM. The viability of cells was controlled by trypan blue staining. Cholesterol content was determined in cell homogenate by an enzymatic method using an Amplex Red Cholesterol kit (Molecular Probes, Eugene, OR) as described by Ostasov et al. [20].

2.4. Detection of eGFP fluorescence in intact cells

Sub-confluent cultures of VTGP cells were grown on glass cover-slips as described above, washed with serum free DMEM and inserted into the chamber of confocal microscope which was pre-equilibrated in 5% CO_2 at 37 °C. The microscope stage was heated to 37 °C. Inverted Leica TCS SP2 AOBS confocal microscope was used for measurement of eGFP fluorescence. The cell sample was excited by 488 nm line of argon laser. When performing cell imaging experiments, the size of the pinhole was set to 1 Airy unit (AU), in order to obtain an optimum signal to noise ratio. In FRAP experiments the size of the pinhole was set to 1.6 AU, so that even a weak signal was detected. In both experiments, the emission was detected in the range from 500 nm to 600 nm. The Plan-Apochromat 100× oil-immersion objective with numerical aperture of 1.4 (also heated to 37 °C) was used.

2.5. The effect of cholesterol depletion on VTGP cell morphology and TRH-R-eGFP distribution

For comparison of changes before and after cholesterol depletion, cells were mounted on the stage of a confocal microscope as described above and 10 mM β-CDX in DMEM was added at time zero. Then, an xyz-series of images of optical sections, encompassing the entire cell depth, was acquired every 5 min. The optical sections were 0.5 μm apart. Results of this primarily methodological recognition are presented in Fig. 1 and described in the Results section (3.1).

2.6. Fluorescence recovery after photobleaching (FRAP)

For comparison of apparent diffusion coefficient (D_{app}) of TRH-R-eGFP molecules before and after cholesterol depletion, FRAP analysis was carried out in the highly fluorescent periphery of the VTGP cells which represents the plasma membrane (Fig. 2). The frames with 12 bit depth of gray and resolution of 512 × 512 pixels (75 × 75 μm) were collected at scanning speed of 800 Hz (870 ms per image). The 50 images of pre-bleach series were collected first. This was followed by 5 iterations of bleach pulses by using 458 nm, 476 nm and 488 nm argon laser lines. For each post-bleach series, 200 images were acquired during 163 s. The data were then extracted from images with ImageJ software version 1.43 m with LOCI Bio-formats importer plug-in. To obtain reliable results and verify that the measured recovery of eGFP fluorescence does not present artificial data, the images were collected from 3 different plasma membrane areas 2, 3, and 6 μm in diameter. Regions smaller than 2 μm could not be analyzed due to the low signal/noise ratio.

Three regions of interest (ROI) were selected and screened in each experiment to obtain the fluorescence intensity signal and proper controls for analysis of a given spot:

- bleached spot of a given size, i.e. 2, 3, and 6 μm in diameter,
- the whole cell area was screened for photobleaching correction,
- background area of the same size as a given bleached spot was selected in the space not occupied by cells and screened as well.

Average intensities for each ROI were then normalized according to Eq. (1) as described by Phair et al. [21]:

$$I_{norm}(t) = \frac{I_{whole(pre)}}{\left(I_{whole}(t) - I_{bgd}(t)\right)} \bullet \frac{\left(I_{bleach}(t) - I_{bgd}(t)\right)}{I_{bleach(pre)}}, \quad (1)$$

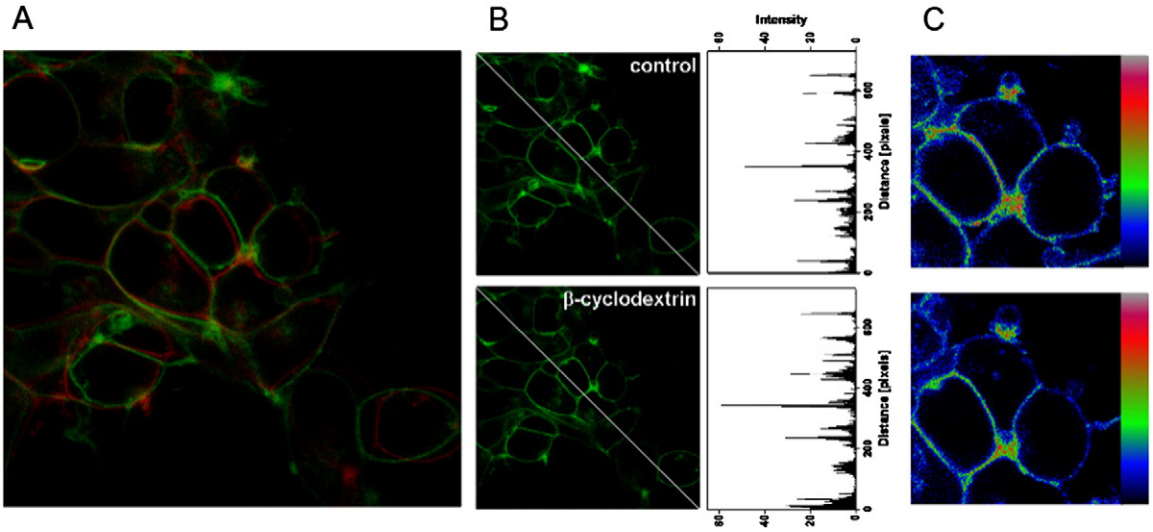

Fig. 1. The effect of cholesterol depletion on cell morphology and TRH-R-eGFP distribution. Left panel (A). Overlay of confocal images of VTGP cells before (green) and after (red) cholesterol depletion. Middle panels (B). Comparison of fluorescence intensity profiles scanned along the line marked in micrographs before (upper) and after (lower panel) cholesterol depletion. Right panels (C). Cut-outs of images shown in B presented in false colors from black (0) to white (255); compare with the scale at the right side of the picture. Note that the intensity of fluorescence is higher at bases of cell processes and in areas where the cells are attached to each other when compared with the remaining areas of the plasma membrane. This type of distribution was not altered by cholesterol depletion — compare β-CDX-untreated (upper) and β-CDX-treated (lower panel) cells.

where

$$I_{whole(pre)} = \frac{\sum_{t_{0-20}}^{t_{0-1}} \left(I_{whole}(t) - I_{bgd}(t)\right)}{20},$$

and

$$I_{bleach(pre)} = \frac{\sum_{t_{0-20}}^{t_{0-1}} \left(I_{bleach}(t) - I_{bgd}(t)\right)}{20}.$$

$I_{bleach}(t)$ is the average intensity within the bleached spot at time t; $I_{bgd}(t)$ is the average intensity within background area at time t; $I_{whole}(t)$ is the average intensity in the whole cell area at time t; t_{0-1} represents the last frame before bleaching and t_{0-20} represents the 20th frame before bleaching.

The mobile fraction of receptor molecules was calculated according to Eq. (2):

$$I_{bleach}(t) = M_f\left(1 - e^{-t\cdot\tau}\right), \quad (2)$$

where M_f is the mobile fraction of receptor molecules and τ characterizes the time needed for maximal recovery of fluorescence intensity in a given spot. For determination of diffusion coefficient, the data were further normalized by using Eq. (3):

$$I_{norm}(t) = \frac{I_{norm}(t) - I_{bleach}(0)}{I_{max} - I_{bleach}(0)}, \quad (3)$$

where $I_{bleach}(0)$ is the normalized fluorescence intensity after the last bleaching pulse.

To obtain apparent diffusion coefficients (D_{app}) these doubly normalized data were fitted with a model considering the two-dimensional diffusion as described by Soumpasis [22] according to Eq. (4):

$$I_{norm}(t) = e^{\frac{-2\tau_D}{t}}\left[I_0\left(\frac{2\tau_D}{t}\right) + I_1\left(\frac{2\tau_D}{t}\right)\right], \quad (4)$$

where τ_D stands for the characteristic diffusion time, i.e., the average time required for the molecule to diffuse across the bleached spot, I_0 and I_1 are modified Bessel functions of a given order. Apparent diffusion coefficient (D_{app}) was then calculated from resulting τ values according to Eq. (5):

$$D_{app} = \frac{\omega^2}{4\tau_D}, \quad (5)$$

where ω is the radius of selected bleached spot.

The time-course of fluorescence recovery was determined in bleached spots of three different sizes: 2 μm (14 control and 12 β-CDX-treated cells), 3 μm (10 control and 10 β-CDX-treated cells) and 6 μm (9 control and 9 β-CDX-treated cells) in diameter, respectively.

Thus, the total number of cells analyzed in this *first* set of FRAP experiments was 64. To obtain satisfactory data from 64 cells, more than 120 cells had to be screened and analyzed because of the errors caused by cell movements and technical problems met in the course of the 6 min span of time required for measurement of a single fluorescence recovery curve. Collection of primary data was performed from confocal planes corresponding to the optical sections through the *M*iddle of the *C*ell (MC mode) using circular ROI placed in the highly fluorescent periphery of the VTGP cells, which represents the plasma membrane (Fig. 2). These circles (of 2-, 3- and 6-μm in diameter) contained the extra- and intracellular spaces around the plasma membrane in roughly the same proportion. This was performed in 5 experiments; finally, the data were processed with MS Excel spreadsheet and GraphPad Prism 4 statistic software.

The methodology described above was subsequently extended in the *second* set of FRAP experiments when the collection of primary data was made from both plasma membrane in MC mode and plasma membrane area in position close to the *G*lass *S*upport (GS mode) as shown in Figs. 5 and 6. For determination of diffusion coefficients, the data were normalized as described before according to Eq. (3). Subsequently, the value of $t_{1/2}$, i.e. the half time of recovery [$I_{norm}(t_{1/2}) = 0.5$], was calculated from the quadratic polynomial fitted to the data with values of $I_{norm}(t)$ in an interval 0–0.8.

To obtain apparent diffusion coefficients (D_{app}) for *circular* spots, the doubly normalized data were calculated using the model considering the two-dimensional diffusion as described by Soumpasis [22] according

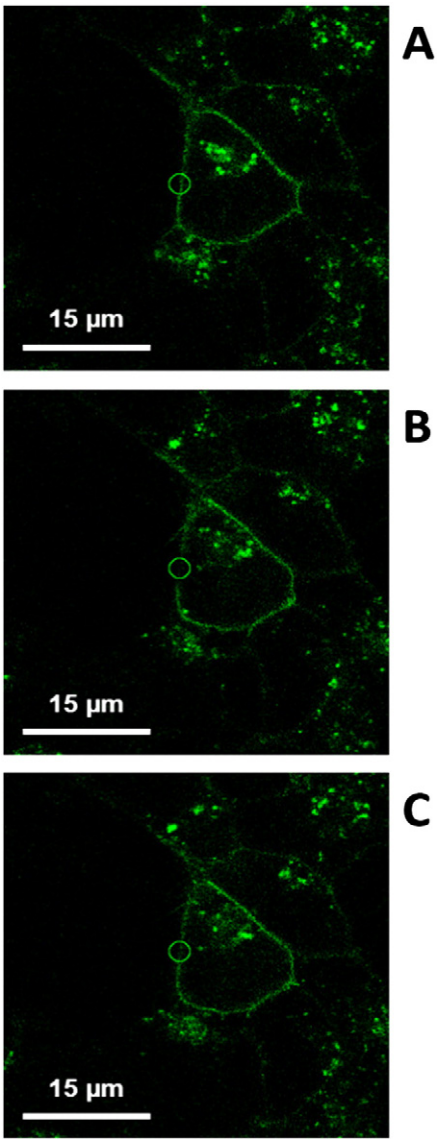

Fig. 2. Confocal microscopy image of VTGP cells in the course of the first set of FRAP experiments. Confocal images of control, β-CDX-untreated VTGP cells showing the same cell before the bleach (A), immediately after the bleach (B) and after maximum recovery of TRH-R-eGFP fluorescence (C). The confocal plane was placed through the cell interior in nearly equatorial position (MC mode). When performing FRAP experiment, the fluorescence signal was monitored in circular area (green circle) representing the 3-μm bleached spot. The results represent the typical FRAP experiment.

to Eq. (4). Apparent diffusion coefficient (D_{app}) was then calculated from the resulting $t_{1/2}$ values according to Eq. (6):

$$D_{app} = 0.224\frac{\omega^2}{t_{1/2}}, \tag{6}$$

where ω is the diameter of the selected bleached spot.

To obtain apparent diffusion coefficients (D_{app}) for *rectangular* spots, the doubly normalized data were calculated using the model considering the two-dimensional diffusion as described by Ellenberg et al. [23] according to Eq. (7):

$$I_{norm}(t) = 1-\sqrt{\frac{\omega^2}{\omega^2 + 4\pi D_{app} t}}. \tag{7}$$

Apparent diffusion coefficient (D_{app}) was then calculated from the resulting $t_{1/2}$ values according to Eq. (8):

$$D_{app} = \frac{\omega^2}{4\pi t_{1/2}}, \tag{8}$$

where ω is the width of the selected bleached spot.

2.7. Raster image correlation spectroscopy (RICS)

RICS is a method providing information on the diffusion and binding of the fluorescently labeled species [24,25]. It is a correlation based approach performed on a set of images, which are collected in confocal microscope equipped with a fast scanning unit. The fluctuations in the fluorescence signal are correlated between different focal positions of the scanner. The temporal delay is then given by the time which the scanner needs for changing its position from one spot to another. Since the signal can be correlated along the lines as well as between the lines and frames, RICS is a versatile method covering the time-scale from tens of microseconds (μs) to seconds (s).

RICS was used for analysis of diffusion of TRH-R-eGFP molecules within the plasma membrane. To achieve this, a model describing diffusion in two dimensions was applied [26]. In this model, correlation for a given position ξ (i) was carried out by function G_S which was calculated as follows:

$$G_S(\xi,\psi) = \frac{\langle \delta I(x,y)\delta I(x+\xi, y+\psi)\rangle_{xy}}{\langle I(x,y)\rangle^2}, \tag{9}$$

where I (x, y) is the fluorescence intensity detected at each pixel and δ I is the fluctuation of the fluorescence intensity around the mean intensity in a given image: $\delta I = I(x,y) - \langle I(x,y)\rangle_{xy}$. The obtained autocorrelation function G_S was then fitted with the formula derived for diffusion in planar systems:

$$G(\xi,\psi) = \frac{\gamma}{N}\left(1 + \frac{4D_{app}\left(\tau_p\xi + \tau_l\psi\right)}{\omega_0^2}\right)^{-1}, \tag{10}$$

where γ accounts for the non-uniform illumination of the excitation volume and is equal to 0.5 for a 2D Gaussian point spread function (PSF), N is the average number of molecules in a given focal volume, D_{app} stands for the diffusion coefficient, ω_0 denotes the lateral waist of the laser beam at the point of focus and τ_p and τ_l stand for pixel dwell time and line scan time, respectively.

Moreover, since the PSF extends over several pixels in the xy-plane, G_S was corrected for scanning itself. The term compensating for fast fluctuations in the brightness of a single molecule was also included in our calculations.

The images were recorded in a confocal Olympus Fluoview 1000 microscope (Olympus, Japan) equipped with a water immersion objective (1.2 NA, 60×). The sample was excited with a 470 nm diode laser LDH-P-C-470 (PicoQuant, Germany) in continuous wave mode. A Q500LP long-pass filter was used in front of the detector. For each RICS experiment, 40 frames consisting of 256 × 256 pixels were collected. The scanner speed along the fast and slow scanning axis was 10 μs/pixel and 3.68 ms/line, respectively. The distance between the scanner steps corresponded to 50 nm, i.e. the overall area of 12.8 × 12.8 μm was scanned for each frame. Photobleaching and slow motions of the sample were ruled out by a moving average subtraction of 4 images for each set of images [25,27]. Before each experiment, the functioning of the setup was confirmed by determination of free Alexa 488 diffusion coefficient in water solution.

2.8. Isolation of plasma membrane fraction in Percoll^R density gradient

VTGP cells were cultivated in 15 flasks (80 cm^2), washed in PBS and harvested by centrifugation for 10 min at 1800 rpm in 50 ml conical vials. The cell pellet was homogenized in 250 mM sucrose, 20 mM Tris–HCl, 3 mM $MgCl_2$, 1 mM EDTA, pH 7.6 plus fresh 1 mM PMSF and complete protease inhibitor cocktail (STEM medium) in loosely-fitting, Teflon-glass homogenizer for 7 min at 1800 rpm. The cell homogenate was centrifuged for 5 min at 1500 rpm for separation of cell debris and nuclear fraction (remaining in the sediment) from post-nuclear supernatant (PNS). The 3 ml volume of PNS was applied on the top of 20 ml of 30% v/v Percoll^R in thick polycarbonate Beckman Ti70 tubes. Centrifugation for 1 h at 27,000 rpm (65,000 × *g*) resulted in separation of two clearly visible layers. The upper layer represented the plasma membrane fraction (PM), the lower layer represented the mitochondria. The upper layer was diluted 1:4 in distilled water and centrifuged in Beckman Ti70 rotor for 2 h at 50,000 rpm (160,000 × *g*). The PM sediment was removed from the compact, gel-like sediment of Percoll^R, re-homogenized by hand in a small volume of 50 mM Tris–HCl, 3 mM $MgCl_2$, 1 mM EDTA, pH 7.4 (TME medium), snap frozen in liquid nitrogen and stored at −80 °C until use. Protein concentration was determined by Lowry method using bovine serum albumin as standard.

2.9. Steady-state fluorescence anisotropy of DPH

Percoll^R-purified PMs were labeled with DPH by the fast addition (under mixing) of 1 mM DPH in freshly distilled acetone to the membrane suspension (1 μM final concentration, 0.1 mg protein/ml). After 30 min at 25 °C, which were allowed to ensure the optimum incorporation of the probe into the membrane [28], the anisotropy of DPH fluorescence was measured at Ex 365 nm/Em 425 nm wavelengths. Under these conditions, the fluorescence intensity of the membrane-bound DPH was ≈500× higher than that of the unbound, free probe in aqueous medium; light scattering problems could be omitted under these conditions. Steady-state fluorescence anisotropy, r_{DPH}, was calculated according to the formula: $r_{DPH} = (I_{vv} - I_{vh}) / (I_{vv} + 2I_{vh})$ according to [29,30].

2.10. The time-resolved fluorescence and dynamic depolarization of DPH

Fluorescence lifetime and polarization experiments were performed in a time correlated single photon counting (TCSPC) spectrofluorometer IBH 5000 U equipped with a cooled Hamamatsu R3809U-50 micro-channel plate photomultiplier detector as described before [31]. The sample was excited at 373 nm with a diode laser (IBH NanoLED-375L, FWHM 80 ps, 1 MHz repetition rate). The emission monochromator was set to 450 nm with slits set to 16 nm. A 400 nm cut-on filter was placed in the emission part of the instrument to reduce a parasitic light from the laser source. The sample was continuously mixed and kept at the constant temperature of 25 °C. The measurement consisted in recording fluorescence decays at 4 different orientations of the emission and excitation polarizers. The anisotropy free decay $I(t)$, which we used for the lifetime determination, was obtained as follows:

$$I(t) = I_{vv}(t) + 2GI_{vh}(t), \tag{11}$$

where I_{vv} is the fluorescence decay measured with both excitation and emission polarized vertically, and I_{vh} with the vertically polarized excitation and horizontally polarized emission. The G-factor (G) was determined by measuring a standard solution of POPOP and calculated as:

$$G = \frac{\langle I_{hv}(t)\rangle_t}{\langle I_{hh}(t)\rangle_t}, \tag{12}$$

where I_{hv} corresponds to the signal measured with horizontally polarized excitation and vertically polarized emission, and I_{hh} to the excitation and emission both polarized horizontally.

In order to obtain fluorescence lifetimes, the $I(t)$ was fitted with two-exponential decay:

$$I(t) = B_1 \exp(-t/\tau_1) + B_2 \exp(-t/\tau_2), \tag{13}$$

yielding lifetimes τ_1 and τ_2 and corresponding amplitudes B_1 and B_2.

The decay of the anisotropy $r(t)$ was determined according to Eq. (14):

$$r(t) = \frac{I_{vv}(t) - GI_{vh}(t)}{I_{vv}(t) + 2GI_{vh}(t)}, \tag{14}$$

and fitted with the formula:

$$r(t) = (r(0) - r(\infty)) \cdot \exp(-t/\phi) + r(\infty), \tag{15}$$

where $r(0)$, and $r(\infty)$ stand for the limiting anisotropy and residual anisotropy, respectively. ϕ, is the rotational correlation time. The anisotropy decays were fitted by the non-linear least squares method including the impulse re-convolution with the instrumental response function (fwhm ~ 100 ps). χ^2 generated by the IBH software package served as a goodness of fit criterion.

The anisotropy data were analyzed according to the "wobble in cone" model introduced by [32,33]. Wobbling diffusion constant (D_w) and S-order parameter were calculated according to Eqs. (16) and (17):

$$D_w = \frac{\sigma_s}{\phi}, \tag{16}$$

$$S = \left(\frac{r(\infty)}{r(0)}\right)^{1/2}, \tag{17}$$

where $r(0)$ and $r(\infty)$ stand for limiting anisotropy and residual anisotropy, ϕ is the rotational correlation time and σ_s is the relaxation time which is a function of the S-order parameter.

2.11 . TRH-stimulated [^{35}S]GTPγS binding

Percoll-purified membranes (20 μg protein per assay) were incubated with (total) or without (basal) increasing concentrations of TRH (10^{-9}–10^{-5} M) in a final volume of 100 μl of reaction mix containing 20 mM HEPES, pH 7.4, 3 mM $MgCl_2$, 100 mM NaCl, 2 μM GDP, 0.2 mM ascorbate and [^{35}S]GTPγS (1 nM, 1250 Ci/mmol) for 30 min at 30 °C. The binding reaction was terminated by dilution with 3 ml of ice-cold 20 mM HEPES (pH 7.4), 3 mM $MgCl_2$, 100 mM NaCl and immediate filtration through Whatman GF/C filters on Brandel cell harvester. Radioactivity remaining on the filters was determined by liquid scintillation using BioScint cocktail. Non-specific GTPγS binding was determined in parallel assays containing 100 μM GTPγS. Binding data were analyzed by GraphPad Prism 4.

When using immunoprecipitation protocol, [^{35}S]GTPγS binding was initiated by the addition of PM to the same assay buffer ± 10 μM TRH including 1 nM [^{35}S]GTPγS, continued for 15 min at 30 °C and terminated by the addition of 0.5 ml of ice cold buffer containing 20 mM HEPES (pH 7.4), 3 mM $MgCl_2$ and 100 mM NaCl. These samples were centrifuged at 16,000 × *g* for 15 min at 4 °C and the resulting pellets were re-suspended in SLB buffer (100 mM Tris, 200 mM NaCl, 1 mM EDTA, 1.25% Nonidet P-40, 0.2% sodium dodecyl sulfate). Samples were precleared with Pansorbin (Calbiochem) and immunoprecipitated with CQ antiserum oriented against C-terminal decapeptide of $G_q/G_{11}\alpha$. Finally, the immuno-complexes were washed twice with solubilization buffer, and bound [^{35}S]GTPγS was determined by liquid-scintillation spectrometry [34].

3. Results

3.1. The effect of cholesterol depletion on VTGP cell morphology and TRH-R-eGFP distribution

Cells grown on glass cover-slips were put on the stage of confocal microscope equipped with a chamber containing 5% CO_2 atmosphere, heated to 37 °C and treated with 10 mM β-CDX for 30 min. Before and during the β-CDX treatment, the "xyz" series of optical sections were acquired throughout the cells every 5 min. The typical picture indicating the detailed VTGP cell morphology and distribution of TRH-R-eGFP molecules is shown in the left panel of Fig. 1(A). This picture was created as an overlay of images acquired before (*green*) and after (*red*) 30 min of β-CDX exposure. Comparison of these images did not indicate any significant change of overall cell morphology or TRH-R-eGFP distribution by cholesterol depletion. In the middle panels of Fig. 1(B), fluorescence intensity profiles were scanned along the line marked in the micrographs; again, these quantitative scans did not reveal any significant difference of receptor distribution before (upper) and after (lower panel) β-CDX exposure.

In the right panels of Fig. 1(C), the cut-outs of images shown in (B) were magnified and presented in false colors. Obviously, the intensity of fluorescence was higher at the bases of cell processes and in areas where the cells were attached to each other than in the remaining areas of the plasma membrane where the receptor distribution was homogeneous, i.e., in bulk membrane phase. Comparison of β-CDX-untreated (C, upper panel) and β-CDX-treated (C, lower panel) cells indicated that this type of distribution, i.e. preferential localization of TRH-R-eGFP at bases of cell processes and sites of cell overlap, was not altered by cholesterol depletion. We could therefore conclude that cholesterol depletion of VTGP cells did not induce any detectable change in distribution of TRH-R-eGFP molecules in the cell membrane, nor in the cell interior. The unchanged VTGP cell morphology was detected in spite of the fact that cholesterol level in homogenate prepared from β-CDX-treated cells was decreased to 68 ± 4% (*, $p < 0.05$) when compared with control, β-CDX-untreated cells (data not shown).

3.2. Confocal laser scanning microscopy of VTGP cells before and in the course of FRAP experiment

Cholesterol depletion causes changes in chemical composition and physical properties of plasma membrane [20,28,35]. These changes should alter the movement of membrane proteins; however, an alteration of membrane structure could be also caused artificially by exposure to the high energy of laser beam. Therefore, confocal images of control (β-CDX-untreated) cells were collected before the bleach (Fig. 2A), immediately after the bleach (Fig. 2B) and at the end of fluorescence recovery phase (Fig. 2C). The small circular area marked ROI indicates the bleached spot of 3 μm in diameter where the data were collected. Comparison of these three types of images indicated that under methodological conditions used in our FRAP experiments (see the next section) the exposure of VTGP cells to the high energy of incoming laser light did not induce any detectable change of the whole cell shape and morphology or structure of plasma (cell) membrane.

3.3. Analysis of TRH-R-eGFP mobility by fluorescence recovery after photobleaching (FRAP)

In the *first* set of FRAP experiments, the time-course of recovery of fluorescence intensity was determined in bleached spots of 2-, 3- and 6 μm in diameter in a total of 64 cells as described in the Materials and methods (Section 2.6). All data were collected from confocal planes corresponding to the optical sections through the *M*iddle of the *C*ells (MC mode) using the circular ROI of the same size as the bleached spot placed in the plasma membrane area. After normalization of data according to Eq. (1) (Fig. 3A–C), the mobile fractions of receptor molecules were calculated according to Eq. (2) (Fig. 3D) and the significance of difference between control (open) and β-CDX-treated (full symbols) cells was analyzed by unpaired Student's t-test. Comparison of mobile fractions (M_f) of TRH-R-eGFP molecules in control and cholesterol-depleted cells did not reveal any significant difference between the two types of cells when analyzed in 2-, 3- and 6-μm spots ($p > 0.05$, NS). Subsequently, the data were normalized according to Eq. (3) (Fig. 4A–C) and for calculation of diffusion coefficients (D_{app}) these doubly normalized data were fitted with a model considering the two-dimensional diffusion as described by Soumpasis [22] (Eq. (4)). The apparent diffusion coefficients (D_{app}) were calculated from the resulting τ values according to Eq. (5) (Section 2.6).

As shown in Fig. 4D and Table 1 (MC mode^{1st}), the obtained apparent diffusion coefficients were virtually the same in 2- and 3-μm spots and not different from each other in control and β-CDX-treated cells. The value of D_{app} in 6 μm spot was much higher than those in the two smaller spots and again, there was no significant difference between control and cholesterol-depleted cells. As far as the large difference between the numerical values of D_{app} determined in 6-μm and two small, 2- and 3-μm spots is concerned, there are two possible explanations based on different sizes of the bleached spots.

First, in small spots (2- and 3-μm), the measured fluorescence intensity is more prone to be affected by i) movement of the cells and ii) inaccuracies arising from introduction of actually unbleached membranes into the recorded position. The probability of occurrence of the second source of error (ii) is less pronounced in the large 6-μm spot, because the entering of the same amount of unbleached, fluorescent membrane into the bleached spot represents a relatively smaller change of the total signal than in 2- and 3-μm spots. Another possible source of error is the diffusion of TRH-R-eGFP molecules proceeding between the last bleaching pulse and the first recording period. Again, this source of error is more probable to occur in smaller spots.

Second, the recovery of fluorescence intensity in a large, 6-μm bleached spot has to be more susceptible to diffusion of fluorescent molecules from the "out of the focus" planes located above and below the confocal plane. Altogether, these interferences and possible sources of error when collecting the primary FRAP data will affect the numerical values of D_{app} even after introduction of the corresponding controls and double-normalization procedure used for calculation of D_{app}.

Therefore, the results of the first set of FRAP experiments performed in 2-, 3- and 6-μm spots, which were based on data collected in MC mode (Table 1, MC mode^{1st}), were verified and extended by the *second* set of FRAP experiments analyzing the 3- and 5-μm spots in the same mode (Table 1, MC mode^{2nd}). However, in this case, data were collected from the following two types of ROI:

- *circles* of 3- or 5-μm in diameter placed at the cell surface containing the extra- and intracellular spaces around the plasma membrane in roughly the same proportions (Figs. 5A, C, and 6A),
- *rectangles* selected within the 3- or 5-μm circles exactly in the plasma membrane area (Fig. 6B) in a similar way as described by Pucadyil and Chattopadhyay [17].

Comparison of the *circle*-based and *rectangle*-based type of analysis indicated that the signal to noise ratio was higher in the latter (rectangles) than in the former (circles) type of analysis (Fig. 6D). Therefore, only the *rectangle*-based analysis was used in the second set of FRAP experiments performed in MC mode (Table 1, MC mode^{2nd}).

We have also collected and analyzed the data from the confocal plane adjacent to the *G*lass *S*upport (Table 1, GS mode). This type of analysis used the circular ROI only because the cell area adjacent to the *G*lass *S*upport was identical with that of the plasma membrane itself. Under these conditions of screening, the whole cell area was shining bright and the signal corresponding to the plasma membrane was

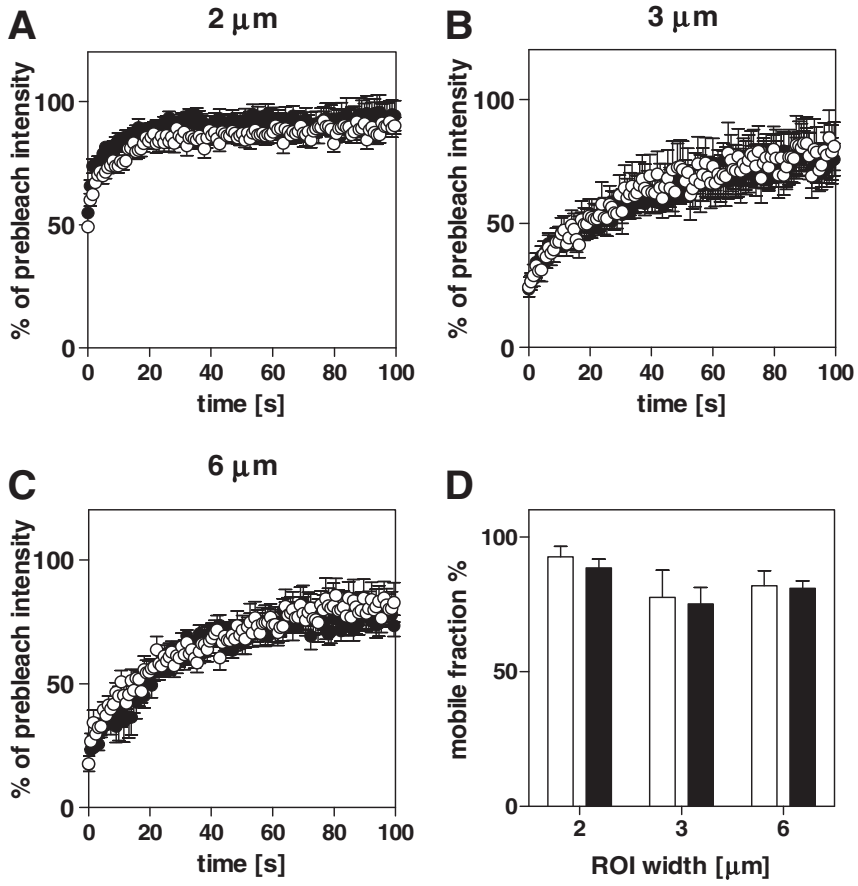

Fig. 3. Averaged records of recovery of TRH-R-eGFP fluorescence in 2- (A), 3- (B) and 6- (C) μm bleached spots and dependence of mobile fraction of receptor molecules on the bleached spot size (D). Fluorescence intensity data were collected in control (β-CDX-untreated) (○) and β-CDX-treated (●) cells before the bleach and in the course of recovery phase of FRAP experiment. The spots of three different widths were analyzed: 2 μm (A), 3 μm (B) and 6 μm (C). Average intensities for each ROI were then normalized according to Eq. (1) as described by Phair et al. [21]. In A (2 μm spot), data represent an average % of pre-bleach intensities collected from 14 control (○) and 12 β-CDX-treated (●) cells; in B (3 μm spot), data represent an average % of pre-bleach intensities collected from 10 control (○) and 10 β-CDX-treated (●) cells; in C (6 μm spot), data represent an average % of pre-bleach intensities collected from 9 control (○) and 9 β-CDX-treated (●) cells. Thus, the time-course of fluorescence recovery was determined in a total of 64 cells. In (D), the mobile fraction of receptor molecules was calculated from the data shown in panels A–C according to Eq. (2) (see Materials and methods). The difference between data collected in control (open columns) and β-CDX-treated (full columns) cells was analyzed by unpaired Student's t-test and found not significant, NS ($p > 0.05$).

identical with the total fluorescence of TRH-R-eGFP molecules determined in the circular ROI of a given size (Figs. 5B, D and 6C).

Collection of primary FRAP data in the *second* set of FRAP experiments, calculation of M_f and D_{app} values and estimation of statistical significance of the difference between the average D_{app} in control and β-CDX-treated cells were performed in a total of 138 cells (Table 1, MC mode^{2nd} and GS mode). As before, the mobile fraction of TRH-R-eGFP molecules was not significantly altered by cholesterol depletion (data not shown). The numerical values of D_{app} were comparable with those determined in 2- and 3-μm spots in the first set of FRAP experiments (MC mode^{1st}). When viewed together, the values of D_{app} were distributed between 0.115 and 0.271 μm^2/s in control cells and between 0.102 and 0.168 μm^2/s in β-CDX-treated cells. Surprisingly, when the doubly-normalized data collected from 5-μm spot, i.e. the $I_{norm}(t)$ values calculated according to Eq. (3), were fitted by quadratic polynomial in an interval 0–0.8, a significant decrease of D_{app} was noticed in cholesterol-depleted cells ($p < 0.01$, Table 1). The same type of analysis in 3-μm spot indicated no difference between the control and β-CDX-treated cells.

When compared with previous literature data, the numerical values of D_{app} determined by us corresponded to the results of other authors (Table 5). The highly significant decrease of D_{app} values by cholesterol depletion was detected for numerous membrane-bound proteins by Kenworthy et al. [36] and Kusumi et al. [37].

3.4. Analysis of TRH-R-eGFP mobility by raster image correlation spectroscopy (RICS)

To verify the results obtained by FRAP analysis, the apparent mobility of TRH-R-eGFP molecules in the plasma membrane of HEK293 cells treated and untreated with β-CDX was determined by raster image correlation spectroscopy (RICS) [24].

RICS represents an up-to-date methodological approach providing information about the movement of fluorescent molecules, which may be used for analysis of diffusion of fluorescent protein molecules within the two-dimensional space of a fluid membrane. This is performed in a set of specifically positioned and quickly screened cell images collected in confocal microscope. RICS was shown to be a complementary method to FRAP [27]. First of all, it is suitable for quantitative characterization of higher speeds of motion (up to ~500 μm^2/s) when compared with FRAP [25]; moreover, it imposes less power on the sample. FRAP, on the other hand, can determine the immobile fraction of the fluorescent molecules, which is eliminated in RICS by subtracting the moving average within a given set of images. Therefore, we found the combination of these two methods as a robust tool for capturing the effect of cholesterol depletion on the TRH-R-eGFP mobility in the plasma membrane.

The depletion of PM cholesterol level by β-CDX changed neither the values of apparent diffusion coefficients determined by RICS, nor the ratio of the amplitudes of the correlation function for the horizontal

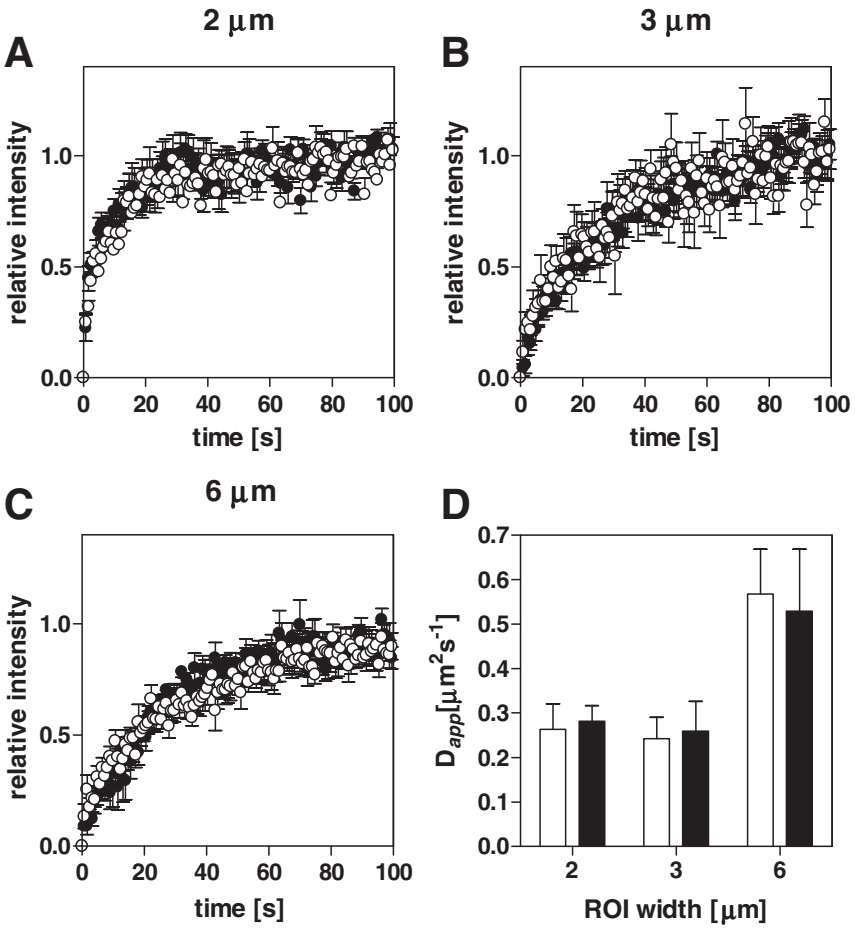

Fig. 4. Normalized records of recovery of TRH-R-eGFP fluorescence (A–C) and dependency of apparent diffusion coefficient on the bleached spot size (D). Fluorescence intensity data presented in Fig. 3A–C were normalized according to Eq. (3) as described in the Materials and methods. Data obtained by analysis of 2 μm (A), 3 μm (B) and 6 μm (C) wide circular spots in control (○) and cholesterol depleted (β-CDX-treated) (●) cells are shown in panels A–C, respectively. In (D), to obtain apparent diffusion coefficients (D_{app}), these doubly normalized data were fitted with a model considering the two-dimensional diffusion as described by Soumpasis [22] according to Eq. (4) using the modified Bessel functions of a given order (see Materials and methods). Finally, the numerical values of D_{app} were calculated according to Eq. (5): $D_{app} = \omega^2 / 4\tau$, where ω is the radius of the given bleach spot. Data represent the average diffusion coefficient ± SEM. The difference between control (open) and β-CDX-treated (full) cells was analyzed by unpaired Student's t-test and found not significant, NS ($p > 0.05$).

and vertical directions in a significant manner (Fig. 7). In contrast to FRAP analysis, the mathematical model applied in RICS is derived for a membrane lying strictly in the focal plane. Therefore, we used data recorded near and in parallel to the *G*lass *S*upport (GS mode) and not in the cell cross-section (MC mode). The obtained results summarized in Table 2 show that cholesterol depletion did not significantly alter the values of D_{app} of TRH-R-eGFP molecules in VTGP plasma membrane. This conclusion opposes the one provided by FRAP for the 5 μm spot. We assume that the evaluation of the RICS data on this longer "length-scale" is not as robust as in the case of FRAP. Therefore, changes in the lateral mobility of TRH-R-eGFP upon cholesterol depletion lie within the experimental error of the method and thus remain undetectable.

The apparent diffusion coefficients D_{app} obtained by RICS were considerably higher than those determined by FRAP (compare Tables 1 and 2). A direct comparison of numerical values of D_{app} determined by these two methods is, however, questionable because quantitative analysis by RICS relies on the assumption that the focal volume is strictly Gaussian. Obviously, this is just a rough approximation in the analysis of plasma membrane of living cells. Furthermore, RICS requires external calibration by aqueous solution containing the fluorescent dye, such as Alexa 488. This represents an additional source of error since the refractive index of the cell interior is different when compared with water. Finally, both RICS and FRAP trace an overall average of all different types of motions/movements proceeding in many smaller compartments of the plasma membrane. Yet, the values of D_{app} obtained by RICS are principally more defined in terms of spatial recognition when compared with FRAP, because collection of primary data in the course of FRAP experiment comprises the non-bleached areas of plasma membrane as well.

3.5. Steady-state fluorescence anisotropy of DPH

Movement of TRH-R-eGFP molecules has to proceed in the hydrophobic lipid matrix of the plasma membrane. Therefore, β-CDX-induced change of "fluidity" of PM isolated from VTGP cells was determined by measurement of steady-state anisotropy of DPH fluorescence (r_{DPH}). Direct exposure of PM to increasing concentrations of β-CDX was reflected in a marked decrease of r_{DPH} values (Table 3A). This indicated an increase of "membrane fluidity". The same result was obtained by measurement of r_{DPH} in PM isolated from control and β-CDX-treated cells (Table 3B). PM prepared from VTGP cells treated with 10 mM β-CDX for 30 min at 37 °C exhibited significantly lower r_{DPH} values than PM prepared from control cells. This decrease was noticed at both temperatures of measurement, 25 °C and 40 °C.

3.6. Studies of hydrophobic plasma membrane interior by dynamic depolarization of DPH fluorescence

Biophysical state of the PM isolated from control and β-CDX-treated cells was also studied by analyzing the time-resolved fluorescence of

Table 1
FRAP analysis: dependence of TRH-R-eGFP diffusion coefficient on the bleached spot size.

ROI μm	Diffusion coefficient ($\mu m^2/s$)		
	Control	+β-CDX	
MC mode[1st] (circle-based analysis)			
2 μm	0.26 ± 0.06 (N = 14)	0.28 ± 0.04 (N = 12)	p > 0.05, NS
3 μm	0.24 ± 0.05 (N = 10)	0.26 ± 0.07 (N = 10)	p > 0.05, NS
6 μm	0.57 ± 0.10 (N = 9)	0.53 ± 0.14 (N = 9)	p > 0.05, NS
MC mode[2nd] (rectangle-based analysis)			
3 μm	0.124 ± 0.009 (N = 15)	0.138 ± 0.031 (N = 19)	p > 0.05, NS
5 μm	0.271 ± 0.022 (N = 19)	0.168 ± 0.012 (N = 17)	p < 0.01
GS mode (circle-based analysis)			
3 μm	0.115 ± 0.011 (N = 19)	0.102 ± 0.006 (N = 17)	p > 0.05, NS
5 μm	0.191 ± 0.009 (N = 16)	0.146 ± 0.012 (N = 16)	p < 0.01

Time-course of fluorescence recovery was determined in bleached spots of three different sizes: 2 μm (14 control and 12 β-CDX-treated cells), 3 μm (10 control and 10 β-CDX-treated cells) and 6 μm (9 control and 9 β-CDX-treated cells) in diameter, respectively.
Thus, the total number of cells analyzed in this *first* set of data was 64.
In the first set of experiments (MC mode[1st]), FRAP analysis was performed in bleached spots of 2-, 3- and 6 μm in diameter as described in the Materials and methods (Section 2.6). All data were collected from confocal planes through the middle part of the cells using the circular ROI of the same size as the bleached spot which was placed in the plasma membrane area (circle-based analysis).
In the second set of experiments, the primary data were collected from 138 cells (69 control and 69 β-CDX-treated) in two types of ROI: *circles* of 3- or 5-μm in diameter placed at the cell surface containing the extra- and intracellular spaces around the plasma membrane in roughly the same proportions (Fig. 6A) and rectangles, which were selected within the 3- or 5-μm circles located exactly in the plasma membrane area (Fig. 6B). Results presented in Table 1 (MC mode[2nd]) were derived from the *rectangle*-based analysis because comparison of the *circle*-based and *rectangle*-based type of analysis indicated that the signal to noise ratio was higher in the latter (rectangles) than in the former (circles) type of analysis (compare with Fig. 6D).
We have also collected and analyzed the data from the confocal plane adjacent to the *G*lass *S*upport (GS mode). This type of analysis used the circular ROI because the cell area adjacent to the *G*lass *S*upport was identical with that of the plasma membrane itself. There was no need for selection of rectangles. Under these conditions of screening, the whole cell area was shining bright and the signal corresponding to the plasma membrane was identical with the total fluorescence of TRH-R-eGFP molecules determined in the circular ROI of a given size (Figs. 5B, D and 6C).
Diffusion coefficients were calculated for each size of the bleached spot and mode of screening as described in the Materials and methods. Data represent the average ± SEM. The difference between control and β-CDX-treated samples was analyzed by unpaired Student's t-test. N, the number of cells analyzed in each mode and a given condition of screening.

DPH in ns range by determination of fluorescence lifetime (τ) and dynamic depolarization of DPH fluorescence [32,33]. Data presented in Table 4 indicated a significant decrease of S-order parameter and increase of wobbling diffusion constant, D_w. This result may be interpreted as increased mobility and more chaotically organized plasma membrane interior in cholesterol-depleted samples of PM. Thus, when combined with the results of the steady-state measurements of DPH fluorescence, cholesterol depletion was reflected in a lower friction of the DPH microenvironment and a higher rate of the DPH rotation.

3.7. Cholesterol depletion attenuates functional coupling of TRH-R-eGFP with the cognate G-proteins of G_q/G_{11} family

In the last part of our work, the intrinsic efficacy of TRH-R-eGFP was determined by high-affinity [^{35}S]GTPγS binding assay (Fig. 8). When using the standard assay conditions, PM isolated from both control (802 ± 46 fmol mg^{-1}) and β-CDX-treated (1112 ± 40 fmol mg^{-1}) cells exhibited a high basal level of binding which was not increased by TRH even at 10^{-5} M concentration (Fig. 8A). This type of result was expected as the attempts to employ standard membrane [^{35}S]GTPγS binding assay to measure activation of G_q/G_{11} family of G proteins by agonist were frequently compromised by the high basal signal to which the G_q/G_{11} G proteins contribute only a small fraction. Under such conditions, significant stimulation of these G proteins is masked by other contributions [38] because the binding of [^{35}S]GTPγS to membranes in the absence of agonists represents a combination of guanine nucleotide exchange proceeding on many different cellular populations of heterotrimeric G proteins together with other proteins (e.g. tubulin) that exchange guanine nucleotides.

Therefore, selection of $G_q/G_{11}\alpha$ proteins from the overall pool of Gα subunits endogenously expressed in HEK293 cells was performed by immuno-precipitation with $G_q/G_{11}\alpha$-oriented antibodies. TRH-stimulated [^{35}S]GTPγS binding was clearly detectable and the net-increment or % of TRH-stimulation was lower in the plasma membranes prepared from cholesterol-depleted cells than from control cells (Fig. 8B). The basal level of [^{35}S]GTPγS binding was drastically decreased in PM prepared from both control (7.3 ± 1.5 fmol mg^{-1}) and β-CDX-treated (6.6 ± 1.3 fmol mg^{-1}) cells and this low level was increased by increasing concentrations of TRH with maximum stimulation (360% of the basal level) at 10^{-5} M TRH. TRH-stimulation was severely attenuated, to 185% of the basal level, in PM isolated from β-CDX-treated cells. We could therefore conclude that the unchanged cholesterol level in PM represents an obligatory condition for optimum functioning of TRH-R-stimulated cascade, namely, for optimum coupling of TRH-R to the cognate G-proteins of G_q/G_{11} family.

4. Discussion

FRAP is an established method for examining the translational mobility of fluorescent molecules in cell membranes [39,40] and, as reviewed in Table 5, this method was intensively used for characterization of the lateral motions of membrane receptor proteins in a variety of cell types. Kenworthy et al. [36] presented results of an extensive FRAP study aiming at clarification of the lipid raft hypothesis. Similarly to our analysis, the apparent diffusion coefficients and fractional mobilities were measured over large areas of PM in circular spots of 4 μm in diameter designed to be much larger than the assumed size of raft regions (<50 nm). FRAP measurements were carried out in COS-7 cells. None of these proteins, however, was a member of 7TM receptor family such as TRH-R-eGFP. Importantly, FRAP measurements performed by Kenworthy et al. [36] were carried out as a function of temperature, cholesterol depletion and cholesterol enrichment.

Cholesterol depletion, performed under almost identical conditions as in our experiments using HEK293 cells (10 mM β-CDX for 30 min), was reflected in a significant *decrease* of apparent diffusion coefficients for both raft and non-raft proteins. The authors concluded that although models in which a small fraction of raft proteins is found in such domains or partitions rapidly between raft and non-raft regions cannot be ruled out, the association with rafts is not the dominant factor governing the overall lateral mobility of membrane proteins. Instead, the apparent diffusion coefficients were much better correlated with the manner in which the proteins were *anchored* to the membrane rather than with their propensity to enter lipid rafts: D_{app} (acylated or prenylated) > D_{app} (GPI-anchored) > D_{app} (transmembrane).

The detailed FRAP analysis of mobility of serotonin$_{1A}$ receptors (5HT-1A), using bleached spots of varying sizes (3-, 4-, 5- and 6-μm in diameter) in control CHO cells [17], was consistent with the models describing diffusion of receptor proteins in a homogeneous membrane. These characteristics were altered in cholesterol-depleted cells in a manner that was consistent with dynamic confinement of receptor molecules in the plasma membrane. Interestingly, the number of specific agonist binding sites was increased by cholesterol depletion in intact cells but decreased in isolated membranes [17].

In this work, we have used CLSM, FRAP and RICS to examine the structural organization and dynamics of motion of TRH-R-eGFP molecules in living HEK293 cells. CLSM analysis did not reveal any change of receptor distribution or intensity of fluorescence signal induced by cholesterol depletion (Fig. 1). Receptor distribution in the plasma membrane was homogeneous under both experimental conditions (± β-CDX) and the intensity of fluorescence localized at the cell surface was unchanged. When discussing this result in the context

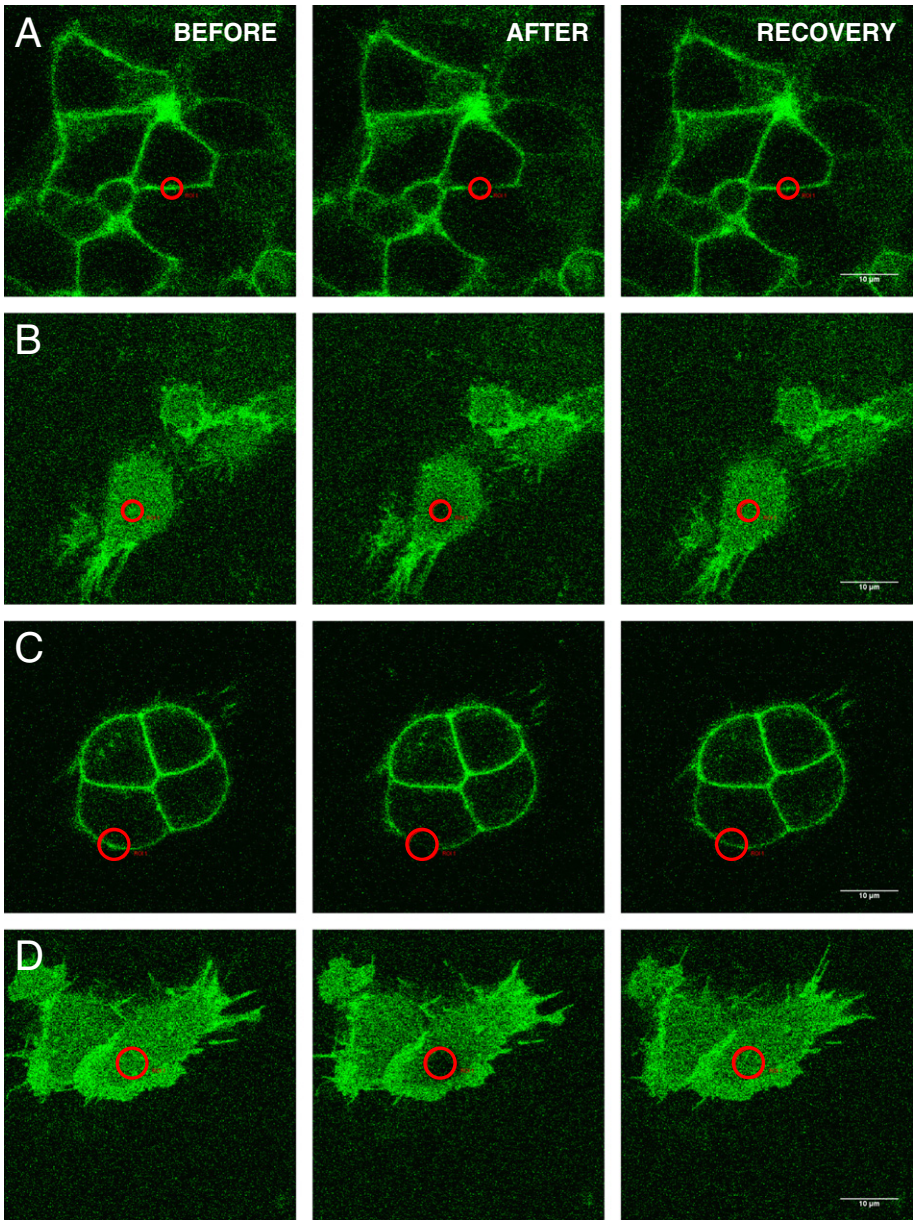

Fig. 5. Confocal microscopy images of VTGP cells in the course of the second set of FRAP experiments; analysis of 3- and 5-μm spots in MC and GS modes. Pictures of the cells and 3-μm bleached spot (red circle) in confocal plane placed through the *M*iddle of the *C*ell (A, MC mode) or in confocal plain situated close to the *G*lass *S*upport (B, GS mode) before the bleach (left), immediately after the bleach (middle) and after recovery of TRH-R-eGFP fluorescence (right). Pictures of the cells and 5-μm bleached spot (red circle) in MC mode (C) or in GS mode (D) before the bleach (left), immediately after the bleach (middle) and after recovery of TRH-R-eGFP fluorescence (right). In order to obtain satisfactory data in GS mode, the confocal plane had to be carefully chosen in an optimum distance from the glass because the data collected from the plane in too close apposition to the glass surface were obscured by the high intensity light scattered from the glass surface. Note please that in GS mode the whole cell area was shining because the TRH-R-eGFP fluorescence signal in the plasma membrane was identical with the signal collected from the cell surface.

of domain-like organization of the cell membrane, this could mean either that a negligible portion of receptor molecules was actually present in membrane domains, or the size of these structures was under the detection limit of our fluorescence microscope.

Fully in line with the simple CLSM screening of VTGP cell morphology, the first set of our FRAP experiments did not reveal any significant alteration of receptor mobility by cholesterol depletion. The mobile fraction of receptor molecules (M_f) determined in bleached spots of different sizes (2-, 3- and 6-μm) was unchanged as the number of mobile receptor molecules expressed as % of the pre-bleach intensity in a given spot was not affected by β-CDX treatment (Fig. 3). The same result was obtained when apparent diffusion coefficients of TRH-R-eGFP molecules (D_{app}) were calculated by fitting the data with model considering a two-dimensional diffusion [22]: there was no significant difference of D_{app} values between the control and cholesterol-depleted cells [Fig. 4 and Table 1 (MC mode^{1st})].

The results of the first set of our FRAP experiments were subsequently extended and verified by an independent analysis of 3 and 5 μm spots which was represented by the new way of collection of primary data, calculation of D_{app} and analysis of statistical significance of differences between control and β-CDX-treated cells [Figs. 5–6 and Table 1 (MC mode^{2nd} and GS mode)]. As before, the mobile fraction of receptor molecules (M_f) was not affected by cholesterol depletion.[1] However, when the doubly-normalized data collected from 5-μm spots were

[1] The absence of an effect of cholesterol depletion on the size of an immobile fraction suggests that the immobile fraction of TRH-R-eGFP molecules in VTGP cells is not generated by recruitment to lipid rafts.

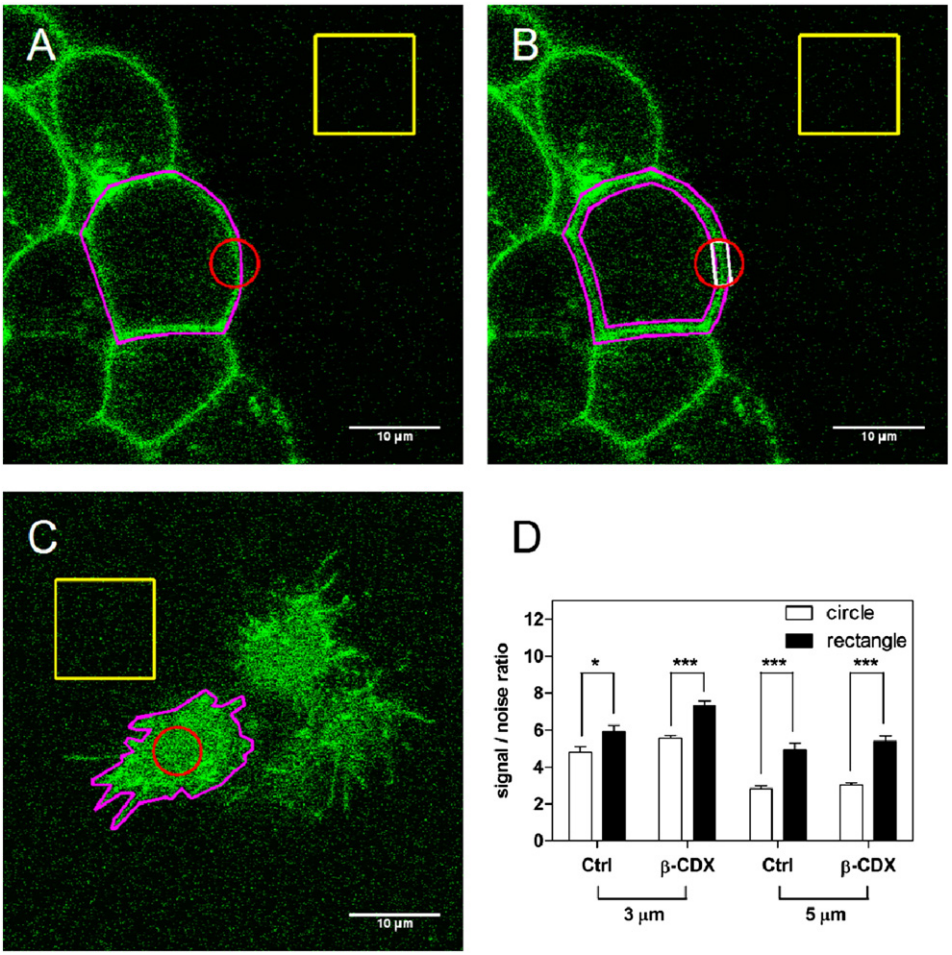

Fig. 6. Methodology of FRAP analysis in the second set of experiments; the circle-based and rectangle-based procedures for collection of primary data from 3- and 5-μm spots. (A, B) Picture of the VTGP cells in confocal plane positioned through the middle part of these cells, i.e., in MC mode. In (A), the 3-μm spot (red circle) containing the extra- and intracellular spaces around the plasma membrane in roughly the same proportions, is shown. The whole cell area (marked by a pink line) was in this case screened for photobleaching correction and the background signal was collected from the extracellular space area marked by the yellow square. In (B), the picture of the same VTGP cell and the same 3-μm spot (red circle) is shown, however, in this case, the rectangular area (white rectangle) was selected within the 3-μm spot so that it was placed directly into the plasma membrane. In this case, the plasma membrane area only (surrounded by a pink line) was screened for the photobleaching correction, i.e., not the whole cell. As in (A), the background signal was collected from the extracellular space area marked by the yellow square. (C) Picture of the different sets of VTGP cells and 3-μm spot (red circle) screened in the confocal plane adjacent to the Glass Support, i.e. in GS mode. As in Fig. 5, the whole cell area was shining because the TRH-R-eGFP signal in the plasma membrane was identical with the signal collected from the cell surface. The whole cell area was screened for photobleaching correction (marked by a pink line) and the background signal was again collected from the yellow square. (D) The signal to noise ratio was calculated for both the circle- (A) and rectangle- (B) based types of analysis of 3-μm and 5-μm spots and expressed as average ± SEM; *, $p < 0.05$; ***, $p < 0.001$. The rectangle-based collection of primary data produced a higher signal to noise ratio when compared with circle-based analysis.

fitted by quadratic polynomial in an interval of 0–0.8, a significant decrease of D_{app} was noticed in cholesterol-depleted cells ($p < 0.01$, Table 1). The same type of analysis in 3-μm spots indicated no difference between control and β-CDX-treated cells.

So, finally, we did obtain a result which was in agreement with data reported by other authors for numerous membrane bound proteins including GPCR [36,37,41] and which may be clearly interpreted in the terms of "corral" or "membrane-skeleton fence" model of plasma membrane organization [37,42]. The difficulties we observed with the detection of alteration of D_{app} values by cholesterol depletion may be attributed to the small amount of TRH-R-eGFP present in membrane domain/raft region of PM under control conditions.

The numerical values of average diffusion coefficients determined by RICS in control and β-CDX-treated cells were higher than those determined by FRAP and *not* significantly different from each other (Fig. 7 and Table 2). This result was similar to that obtained in the *first* set of FRAP experiments (Table 1) and may be explained simply by the high experimental error of these two methodological approaches when applied to the analysis of lateral mobility of receptor molecules proceeding over long distances in large areas of plasma membrane. We assume that the evaluation of the RICS data on the "long-length basis" (5 μm) is not as robust as in the case of an optimum setup and calculation of D_{app} performed in the *second* set of FRAP experiments. The small decrease of lateral mobility of TRH-R-eGFP molecules by cholesterol depletion was lost within the high experimental error of RICS method and remained undetected.

Taken together, the results of FRAP and RICS analyses of VTGP cells were compatible with our previous results [9] indicating a very small amount of TRH-R-eGFP in detergent-resistant membrane domains. When discussing this result, it might be suggested that at high-expression level of TRH-R-eGFP in the cell, the domain-bound pool of receptors would be increased and, consequently, a large change of receptor mobility within the plane of membrane could be noticed [36]. However, under such conditions, it is unlikely that the functional characteristics of TRH-R-eGFP signaling cascade would be comparable to those of TRH-R in native cells [18,19]. The [^{3}H]TRH binding studies performed with VTGP cells indicated the K_d for TRH of 3.8 ± 1.2×10^{-8} M with expression level of 120,000 copies per cell. This expression level was very close to the TRH-R content in GH3 cells, a clonal strain of functional pituitary cells derived from a rat pituitary tumor. GH3 cells endogenously express 130,000 molecules of TRH-R per cell [43].

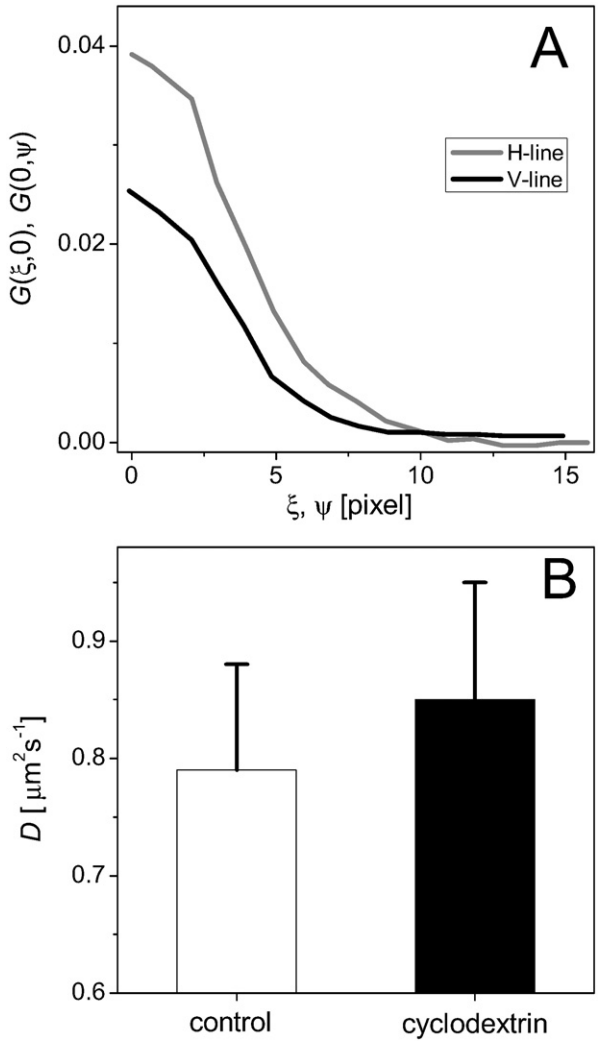

Fig. 7. Raster image correlation spectroscopy (RICS). (A) Cross-sections of the representative autocorrelation function G(ξ, ψ) in the horizontal (along the x-axis) and vertical (along the y-axis) directions. (B) Average diffusion coefficients D ± S.D. in control (open) and β-CDX-treated (full) VTGP cells. The difference between control (open) and β-CDX-treated (full) cells was analyzed by unpaired Student's t-test and found not significant ($p > 0.05$, NS).

We do not exclude the possibility of detection of quantitatively large alteration of TRH-R-eGFP mobility by cholesterol depletion if more suitable biophysical methods were used for analysis of receptor movements. Polarized FRAP can provide information about rotational as opposed to lateral mobility of membrane constituents as it has been reported that rotational motions of membrane proteins and lipid probes are much more sensitive to differences in membrane composition than lateral motions [44–46].

The extensive literature data dealing with the problem of localization of GPCR in membrane domains indicate that some receptors are localized in membrane domains/rafts under control conditions or relocalized into or out of the domains as a consequence of agonist stimulation [47–65]. In the case of δ-OR, cholesterol reduction by methyl-β-CDX attenuated receptor-initiated signaling in neuronal cells but enhanced it in non-neuronal cells [66]. More importantly, δ-OR in resting state was enriched in phosphatidylcholine bilayers, whereas the activated receptor was concentrated in sphingomyelin bilayers characterized by greater thickness [67]. Since it is known that receptor activation involves a change in the orientation of TM helices [68] leading to an increase of receptor vertical length along an axis perpendicular to the plane of the plasma membrane, it was hypothesized that agonist binding redistributed the receptor from phospholipid bilayer to membrane domains enriched in sphingomyelin-enriched bilayer [69]. The driving force for receptor redistribution comes from the increased hydrophobic match of the elongated receptor with the thicker sphingomyelin-enriched bilayer, a sorting mechanism that has previously been observed in other subcellular compartments [70,71]. It was also shown that β_2-ARs are organized in dimeric complexes whose

Table 2
Diffusion coefficients determined by raster image correlation spectroscopy (RICS).

	Diffusion coefficient ($\mu m^2/s$)			
	Control	+β-CDX	N (C, +β-CDX)	p
GS mode	0.79 ± 0.09	0.85 ± 0.10	32, 21	NS, $p > 0.05$

Numbers represent the average value of apparent diffusion coefficient ± SEM. C, control cells; β-CDX, β-CDX-treated cells. N, number of cells analyzed in a given mode. The difference between control and β-CDX-treated samples was analyzed by unpaired Student's t-test and found not significant, NS ($p > 0.05$). The data were collected near the *Glass Support* (GS mode). The excitation light (488 nm) was focused onto the sample in a confocal manner and the emitted light was collected onto the detector. The spatial distribution of the emitted light was considered as Gaussian with the beam waist radius ($1/e^2$) ω_0 of 280 nm. The scanning was performed on the overall area of 12.8 × 12.8 μm in order to gain reasonable statistics on the larger part of the plasma membrane. However, a meaningful correlation was observed within approximately 0.6 μm and 0.4 μm in the horizontal and vertical directions, respectively. The obtained apparent diffusion coefficients are therefore calculated from this region, which is considerably smaller compared to the bleached spots analyzed in FRAP experiments.

Table 3
Steady-state anisotropy of DPH fluorescence.

A. Direct effect of increasing concentrations of β-CDX

β-CDX concentration	r_{DPH} ± SEM
0 mM	0.231 ± 0.005
2.5 mM	0.212 ± 0.008
5 mM	0.194 ± 0.006
10 mM	0.189 ± 0.005

B. Plasma membranes isolated from control and β-CDX-treated VTGP cells

β-CDX concentration	r_{DPH} ± SEM	
	25 °C	40 °C
0 mM	0.216 ± 0.002	0.174 ± 0.002
10 mM	0.203 ± 0.003	0.149 ± 0.003

A. PM prepared from control VTGP cells was exposed to increasing concentrations of β-CDX (2.5, 5 and 10 mM) for 30 min at 25 °C, labeled by DPH (1 μM, 30 min), and r_{DPH} values were determined as described in the Materials and methods. Numbers represent the average ± SEM.
B. VTGP cells were cultivated to 60–70% confluency in 14 flasks (80 cm^2), divided into two portions (7 plus 7 flasks) and either treated (+β-CDX) or untreated (control) with 10 mM β-CDX for 30 min at 37 °C. Subsequently, both β-CDX-treated and control cells were harvested by centrifugation for 10 min at 1800 rpm, snap frozen in liquid nitrogen and stored at −80 °C. To prepare sufficient amount of frozen cell paste for purification of PM, three such cultivation procedures were made. PM was prepared from control (3 × 7 flasks) and β-CDX-treated (3 × 7 flasks) cells by centrifugation in Percoll gradient (2 plus 2 tubes) as described in the Materials and methods.

Table 4
Dynamic depolarization of DPH fluorescence; the time-resolved parameters of DPH fluorescence.

β-CDX (mM)	τ_1	τ_2	r_0	r_∞	ϕ (ns)	S	D_w (ns^{-1})
0	2.87	10.41	0.324	0.186	4.6	0.73	0.022
2.5	2.49	10.08	0.306	0.145	4.6	0.64	0.029
10	1.96	9.42	0.312	0.099	4.9	0.53	0.035

PM isolated from control VTGP cells was exposed to β-CDX (2.5 and 10 mM) for 30 min at 25 °C and labeled by DPH (1 μM, 30 min). Fluorescence lifetime and parameters of time-resolved decays of anisotropy of DPH fluorescence were determined as described in the Materials and methods. τ_1 and τ_2, short and long components of lifetime of DPH fluorescence, r_0, limiting anisotropy at time zero, r_∞, residual anisotropy, ϕ, rotational correlation time, *S*, S-order parameter, D_w, wobbling diffusion constant.

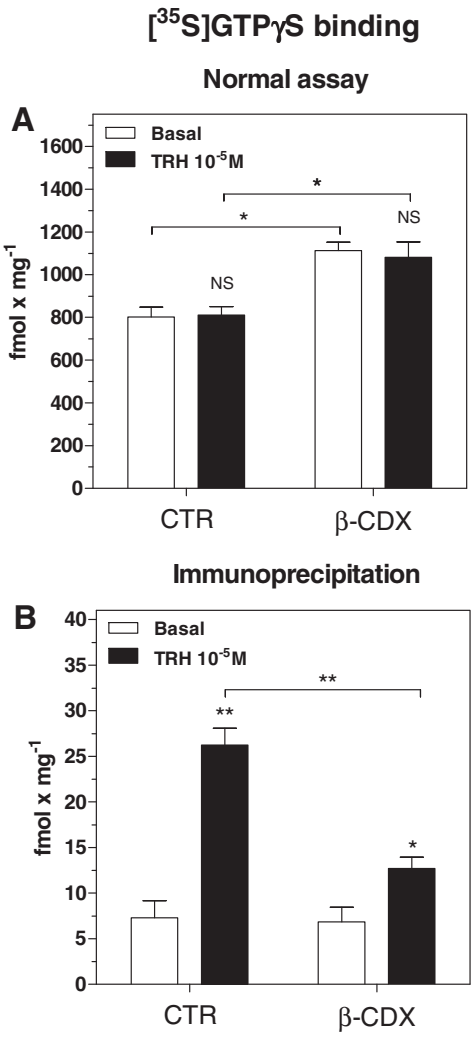

Fig. 8. TRH-stimulated [^{35}S]GTPγS binding in PM isolated from control and β-CDX-treated cells. Stimulation of trimeric G_q/G_{11} G proteins by thyrotropin-releasing hormone (TRH) was measured in plasma membrane fraction (PM) prepared from control and β-CDX-treated VTGP cells by centrifugation in Percoll density gradient. [^{35}S]GTPγS binding assay was measured in reaction mix containing 100 mM NaCl and 2 μM GDP in the absence (□, open columns) or presence (■, full columns) of TRH. Following the experiment, samples were either counted directly (A) or subjected to solubilization in buffer containing 1.25% Nonidet P-40 and 0.2% SDS and immunoprecipitated with CQ antiserum oriented against C-terminal decapeptide of $G_q/G_{11}\alpha$ (B) before scintillation counting (see Materials and methods for more details). Data represent the average ± SEM of 3 independent experiments. The difference between control and β-CDX-treated cells was compared by unpaired Student's t-test; *, **, represent a significant difference, $p < 0.05$, $p < 0.01$, respectively, NS means not significant ($p > 0.05$).

major interactions are mediated by palmitate residues bridged by cholesterol molecules [72].

The abundant literature data presented in the previous paragraph indicate clearly that there is not a general rule which might be used for prediction of the effect of expression level of GPCR on membrane-domain localization and distribution of 7TM proteins between domain-bound and bulk-phase (i.e. detergent-soluble) plasma membrane areas in the context of their physiological function. Obviously, in cells living under optimum conditions in the organism and expressing a physiological level of GPCRs, the domain-bound pool of a given type of GPCR has to be properly controlled and a disturbance of an optimum level has to lead to the alteration of efficiency of signal transmission pathway further down-stream. In this study, the small decrease of receptor mobility by cholesterol depletion (Table 1) was associated with a decrease of efficacy of TRH-stimulated [^{35}S]GTPγS binding to the cognate $G_q/G_{11}\alpha$ proteins (Fig. 8).

Results presented in this work (Tables 1 and 2) together with earlier literature data [36,40] support the view that FRAP method is unlikely to provide unequivocal information about the existence or nonexistence of GPCR in *raft domains* in living cells. Besides the small and highly variable size of these structures [37], the methodological limitations of FRAP have to be considered:

(a) data interpretation depends on the geometric details of the beam shape as well as the fraction of fluorophores initially bleached [39,73],
(b) FRAP is intrinsically macroscopic, ensemble-averaged method that may obscure details arising from putative small, dynamic and submicron lipid rafts. The same applies to RICS.
(c) The lateral mobility of membrane proteins is not sensitive to local viscosity (compare with Tables 3 and 4).

Furthermore, a variety of physiological factors can contribute to the rate and shape of fluorescence recovery. These factors may include transient association with relatively stable membrane components such as cytoskeletal elements, fast membrane traffic between intra- and extracellular space, diffusion barriers, molecular crowding, hydrodynamic interactions, attractive or repulsive nonspecific protein–protein interactions proceeding in the plane of the membrane, local non-planar membrane homologies and local fluctuations in the number of lipid and protein molecules [40].

Visualization of plasma membrane structure in living cell as a dynamic organization of membrane lipids and proteins within i) transient confinement zones (100–300 nm), nanodomains (20–30 nm), small fluid regions and caveolae (50 nm) [74] or ii) "hierarchical and dynamic super-structure" composed of *three-tiered* mesoscale compartments (2–300 nm), raft domains (2–20 nm) and complexes of membrane-associated proteins (3–10 nm) [37,41,42] is compatible with our results because measurements of recovery of TRH-R-eGFP fluorescence were carried out in large areas (7–28 μm^2) of the plasma membrane (Figs. 5 and 6). Therefore, the overall receptor diffusion/mobility represents the average of many different types of motions limited by "hops" from one PM compartment to another. The validity of this statement is best evidenced by the wide range of numerical values of diffusion coefficients of TRH-R-eGFP molecules detected in our FRAP and RICS experiments (Tables 1 and 2) as well as by previous literature data (Table 5).

In the second part of our work, TRH-R-eGFP movement in PM was compared with the well-known effect of cholesterol on the structural and dynamic parameters of the hydrophobic phase of plasma membrane [75]. Cholesterol molecules span approximately half of a bilayer, preferentially interact with the saturated fatty acid chains of phospholipids and, by increasing the packing and lateral assembly of phospholipids, cholesterol reduces membrane fluidity and increases rigidity [76,77]. Fully in line with these literature data, the direct exposure of PM prepared from VTGP cells to increasing concentrations of β-CDX was reflected in a large decrease of anisotropy of the hydrophobic membrane probe DPH (r_{DPH}) from 0.231 ± 0.005 to 0.189 ± 0.005 (Table 3A). The change of r_{DPH} induced by 10 mM β-CDX ($\Delta r_{DPH} = 0.042$) was the same as that induced by heating the membranes from 25 to 40 °C ($\Delta r_{DPH} = 0.042$). Accordingly, PM isolated from β-CDX-treated cells exhibited significantly lower r_{DPH} values than membranes isolated from control cells (Table 3B). Analysis of DPH fluorescence thus documented a dramatic "fluidization" of hydrophobic plasma membrane interior induced by cholesterol depletion.

The interpretation of FRAP and RICS data presented in this work is compatible with our previous biochemical studies of the raft pool of TRH-R in detergent-resistant domains (DRMs) [9]. This pool was very small when compared with the amount of TRH-R in the bulk of plasma membranes, ≈1–3%. As expected, relative content of caveolin and $G_q/G_{11}\alpha$ proteins in DRMs was high, about ≈40%. The difference between TRH-R and 5HT-1A [17] may be simply explained by the large difference

Table 5
Diffusion coefficients of membrane receptors.

Diffusion coefficient	Receptor	Cell type
0.005 $\mu m^2/s$ Axelrod et al. [83]	nAChR, fluorescent α-bungarotoxin	Rat myotubes
0.08 $\mu m^2/s$ Levi et al. [84]	NGFR, fluorescent NGF	Embryonal chicken sensory cells from DRG, PC-12 cells
0.26 $\mu m^2/s$ Poo [85]	nAChR, local inactivation by α-bungarotoxin	*Xenopus* embryonic muscle cells
0.15–0.40 $\mu m^2/s$ Young and Poo [86]	nAChR, local inactivation by α-bungarotoxin	Myotomal muscle cell membrane of *Xenopus* tadpoles
0.4–1.2 $\mu m^2/s$ Barak et al. [87]	β_2-AR GFP fusion protein (β_2-AR/S65T/GFP)	HEK293 cells
0.12–0.16 $\mu m^2/s$ Nelson et al. [88]	GnRHR GFP fusion protein (GnRHR-GFP)	αT3 and CHO cells
0.21 $\mu m^2/s$ Lill et al. [89]	NK1R eGFP fusion protein (eGFP-NK1R)	HEK293 cells
0.18 $\mu m^2/s$ Pucadyil and Chattopadhyay [17]	5-HT_{1A} receptor eYFP fusion protein (5-HT_{1A}-R-eYFP)	CHO cells
0.12–0.27 $\mu m^2/s$ Brejchova, Table 1	TRH-R-eGFP, C-terminus eGFP fusion protein (TRH-R-eGFP)	HEK293 cells

β_2-AR, β_2-adrenergic receptor; CHO, Chinese hamster ovary; DRG, dorsal root ganglion; eGFP, enhanced green fluorescent protein; eYFP, enhanced yellow fluorescent protein; GnRHR, gonadotropin-releasing hormone receptor; HEK, human embryonic kidney; 5-HT, 5-hydroxytryptamine; nAChR, nicotinic acetylcholine receptor; NGF, nerve growth factor; NGFR, nerve growth factor receptor; NK1R, neurokinin 1 receptor; PC-12 cells, pheochromocytoma cell line; TRH-R, thyrotropin-releasing hormone receptor.

in the relative content of these receptors in membrane domains: 1–3% in the case of TRH-R [9] versus 33% for 5HT-1A [78,79].

5. Conclusions

1) The effect of cholesterol depletion on lateral mobility of fully functional TRH-R-eGFP molecules stably expressed in HEK293 cells [18,19] may be interpreted by preferential localization of TRH-R in the bulk of PM which is soluble in non-ionic detergents such as Triton X-100 at 0 °C [9]. The bulk of PM in living cells is composed of *membrane compartments* separated from each other by fences represented by cytoskeleton network attached to the intracellular side of the membrane. Perturbation of PM integrity by cholesterol depletion [9,11] results in the release of a small amount of receptor molecules from rafts into the bulk of plasma membrane. This redistributed pool is difficult to detect because the alteration of an overall mobility of the total receptor population in PM is small when compared to the high experimental error of FRAP and RICS methods applied to the analysis of large areas of PM. Consequently, a significant decrease of D_{app} values by cholesterol depletion may be detected only under special conditions of collection, analysis and calculation of FRAP data.
2) A decrease of PM cholesterol level results in the release of G_q/G_{11}-proteins from membrane domains to the bulk of PM. G_q/G_{11}-proteins are in the resting state present in the domains in high amount and structural order [9,80] and exposed to inhibition by caveolin [81,82]. This may explain why the basal level of [^{35}S]GTPγS binding was increased in PM isolated from cholesterol-depleted cells (Fig. 8A). Here, G proteins randomly meet receptors moving at high speed *within* a given membrane compartment (Tables 1, 2 and 5). The functional coupling of G_q/G_{11} with TRH-R-eGFP proceeds under such (artificial) conditions with lower efficacy than in PM containing intact, properly organized membrane domains (Fig. 8B). Accordingly, the affinity of $G_q/G_{11}\alpha$ response to TRH stimulation was decreased by one order of magnitude in PM isolated from HEK293 cells stably expressing TRH-R and a large amount of $G_{11}\alpha$ [11].
   Similar data were obtained in PM isolated from cholesterol-depleted HEK293 cells stably expressing δ-OR-$G_i1\alpha$ ($C^{351}I$) fusion protein [28]: receptor coupling to both covalently bound, PTX-insensitive $G_i1\alpha$ ($C^{351}I$) and endogenously expressed G_i/G_o proteins proceeded with one order of magnitude lower affinity than in PM prepared from control cells.
3) Fully in line with previous literature data [8,77], degradation of membrane domains by β-CDX treatment resulted in a large increase of "membrane fluidity" of hydrophobic PM interior. This was evidenced by a decrease of steady-state anisotropy of hydrophobic membrane probe DPH (Table 3). More detailed analysis of fluorescence lifetime (τ) and dynamic depolarization of DPH in the same PM indicated a significant decrease of τ, large decrease of residual anisotropy (r_∞) as well as of S-order parameter. Wobbling diffusion constant (D_w) was increased (Table 4). Similar effects of cholesterol depletion on hydrophobic PM matrix were found in HEK293 cells stably expressing δ-OR–$G_i1\alpha$ ($C^{351}I$) fusion protein [28].
4) The unchanged, intact state of plasma membrane represents an obligatory condition for an optimum functioning of TRH-initiated signaling cascade. Distortion of an optimum composition and structural order of PM results in deterioration of the efficacy of coupling between TRH-R and the cognate G_q/G_{11} proteins.

Acknowledgements

This work was supported by the Grant Agency of the Czech Republic (P207/12/0919) and by the Academy of Sciences of the Czech Republic (RVO:67985823). M.H. acknowledges the Praemium Academie Award (Academy of Sciences of the Czech Republic).

References

[1] E. London, D.A. Brown, Insolubility of lipids in Triton X-100: physical origin and relationship to sphingolipid/cholesterol membrane domains (rafts), Biochim. Biophys. Acta Biomembr. 1508 (2000) 182–195.
[2] K. Simons, E. Ikonen, Functional rafts in cell membranes, Nature 387 (1997) 569–572.
[3] K. Simons, E. Ikonen, Cell biology — how cells handle cholesterol, Science 290 (2000) 1721–1726.
[4] D.A. Brown, E. London, Functions of lipid rafts in biological membranes, Annu. Rev. Cell Dev. Biol. 14 (1998) 111–136.
[5] M.P. Lisanti, M. Sargiacomo, P.E. Scherer, Purification of caveolae-derived membrane microdomains containing lipid-anchored signaling molecules such as GPI-anchored proteins, H-Ras, Src-family tyrosine kinases, eNOS, and G-protein alpha-, beta-, and gamma-subunits, Methods Mol. Biol. 116 (1999) 51–60.
[6] R.E. Brown, Sphingolipid organization in biomembranes: what physical studies of model membranes reveal, J. Cell Sci. 111 (1998) 1–9.
[7] R.G.W. Anderson, The caveolae membrane system, Annu. Rev. Biochem. 67 (1998) 199–225.
[8] B. Chini, M. Parenti, G-protein coupled receptors in lipid rafts and caveolae: how, when and why do they go there? J. Mol. Endocrinol. 32 (2004) 325–338.
[9] V. Rudajev, J. Novotny, L. Hejnova, G. Milligan, P. Svoboda, Dominant portion of thyrotropin-releasing hormone receptor is excluded from lipid domains.

Detergent-resistant and detergent-sensitive pools of TRH receptor and G(q)alpha/G(11)alpha protein, J. Biochem. 138 (2005) 111–125.
[10] Z. Moravcova, V. Rudajev, J. Stohr, J. Novotny, J. Cerny, M. Parenti, G. Milligan, P. Svoboda, Long-term agonist stimulation of IP prostanoid receptor depletes the cognate G(s)alpha protein in membrane domains but does not change the receptor level, Biochim. Biophys. Acta, Mol. Cell Res. 1691 (2004) 51–65.
[11] P. Ostasov, L. Bourova, L. Hejnova, J. Novotny, P. Svoboda, Disruption of the plasma membrane integrity by cholesterol depletion impairs effectiveness of TRH receptor-mediated signal transduction via G(q)/G(11)alpha proteins, J. Recept. Signal Transduct. Res. 27 (2007) 335–352.
[12] P. Ostasov, J. Krusek, D. Durchankova, P. Svoboda, J. Novotny, Ca^{2+} responses to thyrotropin-releasing hormone and angiotensin II: the role of plasma membrane integrity and effect of G(11)alpha protein overexpression on homologous and heterologous desensitization, Cell Biochem. Funct. 26 (2008) 264–274.
[13] R.A. Kaiser, B.C. Oxhorn, G. Andrews, I.L.O. Buxton, Functional compartmentation of endothelial P2Y receptor signaling, Circ. Res. 91 (2002) 292–299.
[14] M.E. Lamb, C.W. Zhang, T. Shea, D.J. Kyle, L.M.F. Leeb-Lundberg, Human B1 and B2 bradykinin receptors and their agonists target caveolae-related lipid rafts to different degrees in HEK293 cells, Biochemistry 41 (2002) 14340–14347.
[15] R. Latif, T. Ando, S. Daniel, T.F. Davies, Localization and regulation of thyrotropin receptors within lipid rafts, Endocrinology 144 (2003) 4725–4728.
[16] T.M. Quinton, S. Kim, J. Jin, S.P. Kunapuli, Lipid rafts are required in G alpha(i) signaling downstream of the P2Y12 receptor during ADP-mediated platelet activation, J. Thromb. Haemost. 3 (2005) 1036–1041.
[17] T.J. Pucadyil, A. Chattopadhyay, Cholesterol depletion induces dynamic confinement of the G-protein coupled serotonin (1A) receptor in the plasma membrane of living cells, Biochim. Biophys. Acta Biomembr. 1768 (2007) 655–668.
[18] T. Drmota, G.W. Gould, G. Milligan, Real time visualization of agonist-mediated redistribution and internalization of a green fluorescent protein-tagged form of the thyrotropin-releasing hormone receptor, J. Biol. Chem. 273 (1998) 24000–24008.
[19] T. Drmota, J. Novotny, G.W. Gould, P. Svoboda, G. Milligan, Visualization of distinct patterns of subcellular redistribution of the thyrotropin-releasing hormone receptor-1 and G(q)alpha/G(11)alpha induced by agonist stimulation, Biochem. J. 340 (1999) 529–538.
[20] P. Ostasov, J. Sykora, J. Brejchova, A. Olzynska, M. Hof, P. Svoboda, FLIM studies of 22- and 25-NBD-cholesterol in living HEK293 cells: plasma membrane change induced by cholesterol depletion, Chem. Phys. Lipids 167 (2013) 62–69.
[21] R.D. Phair, S.A. Gorski, T. Misteli, Measurement of dynamic protein binding to chromatin in vivo, using photobleaching microscopy, Methods Enzymol. 375 (2004) 393–414.
[22] D.M. Soumpasis, Theoretical analysis of fluorescence photobleaching recovery experiments, Biophys. J. 41 (1983) 95–97.
[23] J. Ellenberg, E.D. Siggie, J.E. Moreira, C.L. Smith, J.F. Presely, H.J. Worman, J. Lippincott-Schwartz, Nuclear membrane dynamics and reassembly in living cells: targeting of inner nuclear membrane protein in interphase and mitosis, J. Cell Biol. 138 (1997) 1193–1206.
[24] M.A. Digman, E. Gratton, Analysis of diffusion and binding in cells using the RICS approach, Microsc. Res. Tech. 72 (2009) 323–332.
[25] M.J. Rossow, J.M. Sasaki, M.A. Digman, E. Gratton, Raster image correlation spectroscopy in live cells, Nat. Protoc. 5 (2010) 1761–1774.
[26] E. Gielen, N. Smisdom, M. vandeVen, B. De Clercq, E. Gratton, M. Digman, J.M. Rigo, J. Hofkens, Y. Engelborghs, M. Ameloot, Measuring diffusion of lipid-like probes in artificial and natural membranes by raster image correlation spectroscopy (RICS): use of a commercial laser-scanning microscope with analog detection, Langmuir 25 (2009) 5209–5218.
[27] S.C.P. Norris, J. Humpolickova, E. Amler, M. Huranova, M. Buzgo, R. Machan, D. Lukas, M. Hof, Raster image correlation spectroscopy as a novel tool to study interactions of macromolecules with nanofiber scaffolds, Acta Biomater. 7 (2011) 4195–4203.
[28] J. Brejchova, J. Sykora, K. Dlouha, L. Roubalova, P. Ostasov, M. Vosahlikova, M. Hof, P. Svoboda, Fluorescence spectroscopy studies of HEK293 cells expressing DOR-G(i)1 alpha fusion protein; the effect of cholesterol depletion, Biochim. Biophys. Acta Biomembr. 1808 (2011) 2819–2829.
[29] M. Shinitzky, Y. Barenholz, Dynamics of the hydrocarbon layer in liposomes of lecithin and sphingomyelin containing dicetylphosphate, J. Biol. Chem. 249 (1974) 2652–2657.
[30] M. Shinitzky, Y. Barenholz, Fluidity parameters of lipid regions determined by fluorescence polarization, Biochim. Biophys. Acta 515 (1978) 367–394.
[31] J. Sykora, L. Bourova, M. Hof, P. Svoboda, The effect of detergents on trimeric G-protein activity in isolated plasma membranes from rat brain cortex: correlation with studies of DPH and Laurdan fluorescence, Biochim. Biophys. Acta Biomembr. 1788 (2009) 324–332.
[32] S. Kawato, K. Kinosita, A. Ikegami, Dynamic structure of lipid bilayers studied by nanosecond fluorescence techniques, Biochemistry 16 (1977) 2319–2324.
[33] K. Kinosita, A. Ikegami, S. Kawato, On the wobbling-in-cone analysis of fluorescence anisotropy decay, Biophys. J. 37 (1982) 461–464.
[34] J. Novotny, D. Durchankova, R.J. Ward, J.J. Carrillo, P. Svoboda, G. Milligan, Functional interactions between the alpha(1b)-adrenoceptor and G alpha(11) are compromised by de-palmitoylation of the G protein but not of the receptor, Cell. Signal. 18 (2006) 1244–1251.
[35] E. Ikonen, Cellular cholesterol trafficking and compartmentalization, Nat. Rev. Mol. Cell Biol. 9 (2008) 125–138.
[36] A.K. Kenworthy, B.J. Nichols, C.L. Remmert, G.M. Hendrix, M. Kumar, J. Zimmerborg, J. Lippincott-Schwartz, Dynamics of putative raft-associated proteins at the cell surface, J. Cell Biol. 165 (2004) 735–746.
[37] A. Kusumi, K.G.N. Suzuki, R.S. Kasai, K. Ritchie, T.K. Fujiwara, Hierarchical mesoscale domain organization of the plasma membrane, Trends Biochem. Sci. 36 (2010) 604–615.
[38] G. Milligan, Principles: extending the utility of [^{35}S]GTP gamma S binding assays, Trends Pharmacol. Sci. 24 (2003) 87–90.
[39] D. Axelrod, D.E. Koppel, J. Schlessinger, E. Elson, W.W. Webb, Mobility measurement by analysis of fluorescence photobleaching recovery kinetics, Biophys. J. 16 (1976) 1055–1069.
[40] B.K. Lagerholm, G.E. Weinreb, K. Jacobson, N.L. Thompson, Detecting microdomains in intact cell membranes, Annu. Rev. Phys. Chem. 56 (2005) 309–336.
[41] K. Suzuki, K. Ritchie, E. Kajikawa, T. Fujiwara, A. Kusumi, Rapid hop diffusion of a G-protein-coupled receptor in the plasma membrane as revealed by single-molecule techniques, Biophys. J. 88 (2005) 3659–3680.
[42] A. Kusumi, Y. Sako, Cell surface organization by the membrane skeleton, Curr. Opin. Cell Biol. 8 (1996) 566–574.
[43] P.M. Hinkle, A.H. Tashjian, Receptors for thyrotropin-releasing hormone in prolactin producing rat pituitary cells in culture, J. Biol. Chem. 248 (1973) 6180–6186.
[44] M. Velez, D. Axelrod, Polarized fluorescence photobleaching recovery for measuring rotational diffusion in solutions and membranes, Biophys. J. 53 (1988) 575–591.
[45] M.M. Timbs, N.L. Thopson, Slow rotational mobilities of antibodies and lipids associated with substrate-supported phospholipid monolayers as measured by polarized fluorescence photobleaching recovery, Biophys. J. 58 (1990) 413–428.
[46] R.K.P. Benninger, B. Onfelt, M.A.A. Neil, D.M. Davis, P.M.W. French, Fluorescence imaging of two-photon linear dichroism: cholesterol depletion disrupts molecular orientation in cell membranes, Biophys. J. 88 (2005) 609–622.
[47] T. Sabourin, L. Bastien, D.R. Bachvarov, F. Marceau, Agonist-induced translocation of the kinin B-1 receptor to caveolae-related rafts, Mol. Pharmacol. 61 (2002) 546–553.
[48] G. Raposo, E.L. Benedetti, Are beta-ARs internalized via caveolae or coated pits? Trends Cell Biol. 4 (1994) 418.
[49] G. Raposo, I. Dunia, C. Delavierklutchko, S. Kaveri, A.D. Strosberg, E.L. Benedetti, Internalization of beta-adrenergic receptor in A431 cells involves non-coated vesicles, Eur. J. Cell Biol. 50 (1989) 340–352.
[50] R.D. Lasley, P. Narayan, A. Uittenbogaard, E.J. Smart, Activated cardiac adenosine A(1) receptors translocate out of caveolae, J. Biol. Chem. 275 (2000) 4417–4421.
[51] W.F.C. De Weerd, L.M.F. Leeb-Lundberg, Bradykinin sequesters B2 bradykinin receptors and the receptor-coupled G alpha subunits G alpha(q) and G alpha(1) in caveolae, FASEB J. 11 (1997) (A1328-A1328).
[52] O. Feron, T.W. Smith, T. Michel, R.A. Kelly, Dynamic targeting of the agonist-stimulated m2 muscarinic acetylcholine receptor to caveolae in cardiac myocytes, J. Biol. Chem. 272 (1997) 17744–17748.
[53] R.S. Ostrom, S.R. Post, P.A. Insel, Stoichiometry and compartmentation in G protein-coupled receptor signaling: implications for therapeutic interventions involving G(s), J. Pharmacol. Exp. Ther. 294 (2000) 407–412.
[54] K.S. Murthy, G.M. Makhlouf, Heterologous desensitization mediated by G protein-specific binding to caveolin, J. Biol. Chem. 275 (2000) 30211–30219.
[55] C. Dessy, R.A. Kelly, J.L. Balligand, O. Feron, Dynamin mediates caveolar 2 sequestration of muscarinic cholinergic receptors and alteration in NO signaling, EMBO J. 19 (2000) 4272–4280.
[56] J. Igarashi, T. Michel, Agonist-modulated targeting of the EDG-1 receptor to plasmalemmal caveolae–eNOS activation by sphingosine 1-phosphate and the role of caveolin-1 in sphingolipid signal transduction, J. Biol. Chem. 275 (2000) 32363–32370.
[57] V.O. Rybin, E. Pak, S. Alcott, S.F. Steinberg, Developmental changes in beta(2)-adrenergic receptor signaling in ventricular myocytes: the role of Gi proteins and caveolae microdomains, Mol. Pharmacol. 63 (2003) 1338–1348.
[58] V.O. Rybin, X.H. Xu, M.P. Lisanti, S.F. Steinberg, Differential targeting of beta-adrenergic receptor subtypes and adenylyl cyclase to cardiomyocyte caveolae — a mechanism to functionally regulate the cAMP signaling pathway, J. Biol. Chem. 275 (2000) 41447–41457.
[59] M. Ushio-Fukai, L. Hilenski, N. Santanam, P.L. Becker, Y.X. Ma, K.K. Griendling, R.W. Alexander, Cholesterol detection inhibits epidermal growth factor receptor transactivation by angiotensin II in vascular smooth muscle cells — role of cholesterol-rich microdomains and focal adhesions in angiotensin II signaling, J. Biol. Chem. 276 (2001) 48269–48275.
[60] R.S. Ostrom, P.A. Insel, The evolving role of lipid rafts and caveolae in G protein-coupled receptor signaling: implications for molecular pharmacology, Br. J. Pharmacol. 143 (2004) 235–245.
[61] A. Becher, A. Green, A.O. Ige, A. Wise, J.H. White, R.A.J. McIlhinney, Ectopically expressed gamma-aminobutyric acid receptor B is functionally down-regulated in isolated lipid raft-enriched membranes, Biochem. Biophys. Res. Commun. 321 (2004) 981–987.
[62] M. Karlsson, H. Thorn, A. Danielsson, K.G. Stenkula, A. Ost, J. Gustavsson, F.H. Nystrom, P. Stralfors, Colocalization of insulin receptor and insulin receptor substrate-1 to caveolae in primary human adipocytes — cholesterol depletion blocks insulin signalling for metabolic and mitogenic control, Eur. J. Biochem. 271 (2004) 2471–2479.
[63] M. Bari, N. Battista, F. Fezza, A. Finazzi-Agro, M. Maccarrone, Lipid rafts control signaling of type-1 cannabinoid receptors in neuronal cells — implications for anandamide-induced apoptosis, J. Biol. Chem. 280 (2005) 12212–12220.
[64] W. Xu, S.I. Yoon, P. Huang, Y.L. Wang, C.G. Chen, P.L.G. Chong, L.Y. Liu-Chen, Localization of the kappa opioid receptor in lipid rafts, J. Pharmacol. Exp. Ther. 317 (2006) 1295–1306.
[65] J.A. Allen, R.A. Halverson-Tamboli, M.M. Rasenick, Lipid raft microdomains and neurotransmitter signalling, Nat. Rev. Neurosci. 8 (2007) 128–140.
[66] P. Huang, W. Xu, S.I. Yoon, C.G. Chen, P.L.G. Chong, L.Y. Liu-Chen, Cholesterol reduction by methyl-beta-cyclodextrin attenuates the delta opioid receptor-mediated signaling in neuronal cells but enhances it in non-neuronal cells, Biochem. Pharmacol. 73 (2007) 534–549.

[67] I.D. Alves, Z. Salamon, V.J. Hruby, G. Tollin, Ligand modulation of lateral segregation of a G-protein-coupled receptor into lipid microdomains in sphingomyelin/phosphatidylcholine solid-supported bilayers, Biochemistry 44 (2005) 9168–9178.
[68] U. Gether, B.K. Kobilka, G protein-coupled receptors — II. Mechanism of agonist activation, J. Biol. Chem. 273 (1998) 17979–17982.
[69] Z. Salamon, S. Cowell, E. Varga, H.I. Yamamura, V.J. Hruby, G. Tollin, Plasmon resonance studies of agonist/antagonist binding to the human delta-opioid receptor: new structural insights into receptor-ligand interactions, Biophys. J. 79 (2000) 2463–2474.
[70] M.O. Jensen, O.G. Mouritsen, Lipids do influence protein function — the hydrophobic matching hypothesis revisited, Biochim. Biophys. Acta Biomembr. 1666 (2004) 205–226.
[71] A.G. Lee, How lipids affect the activities of integral membrane proteins, Biochim. Biophys. Acta Biomembr. 1666 (2004) 62–87.
[72] V. Cherezov, D.M. Rosenbaum, M.A. Hanson, S.G.F. Rasmussen, F.S. Thian, T.S. Kobilka, H.J. Choi, P. Kuhn, W.I. Weis, B.K. Kobilka, R.C. Stevens, High-resolution crystal structure of an engineered human beta(2)-adrenergic G protein-coupled receptor, Science 318 (2007) 1258–1265.
[73] J. Lippincott-Schwartz, E. Knapp, A. Kenworthy, Studying protein dynamics in living cells, Nat. Rev. Cell Biol. 2 (2001) 444–456.
[74] F.R. Maxfield, Plasma membrane microdomains, Curr. Opin. Cell Biol. 14 (2002) 483–487.
[75] M. Shinitzky, Membrane fluidity and cellular functions, in: M. Shinitzky (Ed.), Physiology of Membrane Fluidity, CRC Press, Boca Raton, 1984, pp. 1–51.
[76] O.G. Mouritsen, M.J. Zuckermann, What's so special about cholesterol? Lipids 39 (2004) 1101–1113.
[77] B. Chini, M. Parenti, G-protein-coupled receptors, cholesterol and palmitoylation: facts about fats, J. Mol. Endocrinol. 42 (2009) 371–379.
[78] S. Kalipatnapu, A. Chattopadhyay, Membrane organization of the human serotonin(1A) receptor monitored by detergent insolubility using GFP fluorescence, Mol. Membr. Biol. 22 (2005) 539–547.
[79] U. Renner, K. Glebov, T. Lang, E. Papusheva, S. Balakrishnan, B. Keller, D.W. Richter, R. Jahn, E. Ponimaskin, Localization of the mouse 5-hydroxytryptamine(1A) receptor in lipid microdomains depends on its palmitoylation and is involved in receptor-mediated signaling, Mol. Pharmacol. 72 (2007) 502–513.
[80] P. Oh, J.E. Schnitzer, Segregation of heterotrimeric G proteins in cell surface microdomains. G(q) binds caveolin to concentrate in caveolae, whereas G(i) and G(s) target lipid rafts by default, Mol. Biol. Cell 12 (2001) 685–698.
[81] R.M. Epand, B.G. Sayer, R.F. Epand, Caveolin scaffolding region and cholesterol-rich domains in membranes, J. Mol. Biol. 345 (2005) 339–350.
[82] R.F. Epand, A. Thomas, R. Brasseur, S.A. Vishwanathan, E. Hunter, R.M. Epand, Juxtamembrane protein segments that contribute to recruitment of cholesterol into domains, Biochemistry 45 (2006) 6105–6114.
[83] D. Axelrod, P. Ravdin, D.E. Koppel, J. Schlessinger, W.W. Webb, E.L. Elson, T.R. Podleski, Lateral motion of fluorescently labeled acetylcholine receptors in membranes of developing muscle fibers, Proc. Natl. Acad. Sci. U. S. A. 73 (1976) 4594–4598.
[84] A. Levi, Y. Shechter, E.J. Neufeld, J. Schlessinger, Mobility, clustering, and transport of nerve growth factor in embryonal sensory cells and in a sympathetic neuronal cell line, Proc. Natl. Acad. Sci. U. S. A. 77 (1980) 3469–3473.
[85] M.M. Poo, Rapid lateral diffusion of functional Ach receptors in embryonic muscle cell membrane, Nature 295 (1982) 332–334.
[86] S.H. Young, M.M. Poo, Rapid lateral diffusion of extrajunctional acetylcholine receptors in the developing muscle membrane of *Xenopus* tadpole, J. Neurosci. 3 (1983) 225–231.
[87] L.S. Barak, S.S.G. Ferguson, J. Zhang, C. Martenson, T. Meyer, M.G. Caron, Internal trafficking and surface mobility of a functionally intact beta(2)-adrenergic receptor-green fluorescent protein conjugate, Mol. Pharmacol. 51 (1997) 177–184.
[88] S. Nelson, R.D. Horvat, J. Malvey, D.A. Roess, B.G. Barisas, C.M. Clay, Characterization of an intrinsically fluorescent gonadotropin-releasing hormone receptor and effects of ligand binding on receptor lateral diffusion, Endocrinology 140 (1999) 950–957.
[89] Y. Lill, K.L. Martinez, M.A. Lill, B.H. Meyer, H. Vogel, B. Hecht, Kinetics of the initial steps of G protein-coupled receptor-mediated cellular signaling revealed by single-molecule imaging, ChemPhysChem 6 (2005) 1633–1640.